iScience

CellPress
OPEN ACCESS

Article

Erythropoietin Regulates Transcription and YY1 Dynamics in a Pre-established Chromatin Architecture

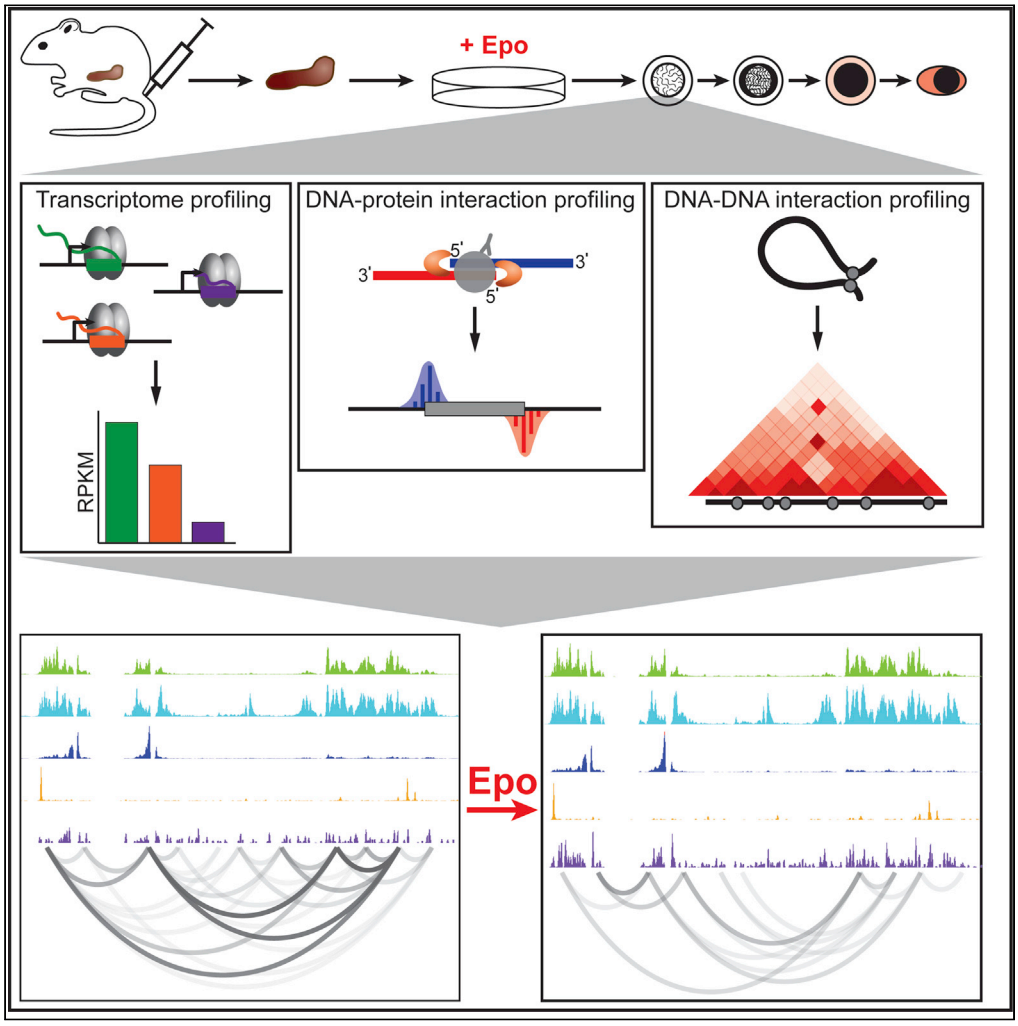

Andrea A. Perreault, Jonathan D. Brown, Bryan J. Venters

andrea.a.perreault@vanderbilt.edu (A.A.P.)
bjventers@gmail.com (B.J.V.)

HIGHLIGHTS

EPO induces rapid RNA Pol II response at a key subset of genes

YY1 is redistributed in the genome following 1 h EPO stimulation

CTCF and YY1 bind different locations pre and post 1 h EPO stimulation

E-P loops mediated by H3K27ac are largely invariant in response to EPO

Perreault et al., iScience *23*, 101583
October 23, 2020
https://doi.org/10.1016/j.isci.2020.101583

iScience

CellPress
OPEN ACCESS

Article

Erythropoietin Regulates Transcription and YY1 Dynamics in a Pre-established Chromatin Architecture

Andrea A. Perreault,[1,3,4,*] Jonathan D. Brown,[2,3] and Bryan J. Venters[3,*]

SUMMARY

The three-dimensional architecture of the genome plays an essential role in establishing and maintaining cell identity. However, the magnitude and temporal kinetics of changes in chromatin structure that arise during cell differentiation remain poorly understood. Here, we leverage a murine model of erythropoiesis to study the relationship between chromatin conformation, the epigenome, and transcription in erythroid cells. We discover that acute transcriptional responses induced by erythropoietin (EPO), the hormone necessary for erythroid differentiation, occur within an invariant chromatin topology. Within this pre-established landscape, Yin Yang 1 (YY1) occupancy dynamically redistributes to sites in proximity of EPO-regulated genes. Using HiChIP, we identify chromatin contacts mediated by H3K27ac and YY1 that are enriched for enhancer-promoter interactions of EPO-responsive genes. Taken together, these data are consistent with an emerging model that rapid, signal-dependent transcription occurs in the context of a pre-established chromatin architecture.

INTRODUCTION

Transcription control is a primary mechanism for regulating gene expression in eukaryotes. Three major steps exist in the transcription cycle: (1) preinitiation complex (PIC) formation, (2) pause release of RNA polymerase II (Pol II) to productive elongation, and (3) transcription termination (Liu et al., 2015). Multiple mechanisms exist to regulate each step, thereby providing precise control over the magnitude and kinetics of transcription and global gene expression. Promoter proximal pausing is one such mechanism and is recognized as a general feature of transcription at many eukaryotic genes. Specifically, there is a prominence of paused Pol II at signal-responsive genes, which serves to prime these genes for rapid transcription in response to environmental stimuli (Adelman et al., 2009; Gaertner et al., 2012; Danko et al., 2013). Transcription factor (TF)-bound enhancers activate Pol II, acting as an additional mechanism in regulating transcription (Heintzman et al., 2009) and defining cell identity (Ernst et al., 2011; Zhu et al., 2013). Athough chromatin state maps are useful to assign enhancers to target genes based on distance from promoters, proximity analysis is overly simplistic with respect to the true gene regulatory environment (Mora et al., 2016; Yao et al., 2015; Rao et al., 2014).

More recently, high-resolution maps of the three-dimensional (3D) genome have revealed that enhancers exhibit long-range control of transcription. Structural proteins, such as CCCTC-binding factor (CTCF) and Yin Yang 1 (YY1), tether distal TF-bound enhancers to their target gene promoters. CTCF is an evolutionarily conserved zinc finger that co-localizes with cohesin (Phillips and Corces, 2009). Together, these two factors establish and maintain chromatin loops (Sanyal et al., 2012; Rao et al., 2017; Ren et al., 2017). Assays that can map chromatin contacts, such as HiC, have revealed that the genome is organized into topologically associated domains (TADs), which are demarcated by CTCF (Lieberman-Aiden et al., 2009; Dixon et al., 2012) and are largely consistent between cell types (Phillips and Corces, 2009; Ong and Corces, 2014; Arzate-Mejia et al., 2018). These large domains can be further separated into subTADs that contain higher contact frequencies between regions of the genome, many of which are not limited to one-to-one interactions (Li et al., 2012; Sanyal et al., 2012; Fullwood et al., 2009; Dowen et al., 2014; Ji et al., 2016). Together, these findings demonstrate CTCF's function as structural foci for chromatin organization, whereby Pol II can selectively target cell-type-specific genes for transcription through interactions with looping factors and enhancers.

[1]Chemical and Physical Biology Program, Vanderbilt University, Nashville, TN 37232, USA

[2]Division of Cardiovascular Medicine, Department of Medicine, Vanderbilt University Medical Center, Nashville, TN 37232, USA

[3]Molecular Physiology and Biophysics, Vanderbilt University, Nashville, TN 37232, USA

[4]Lead Contact

*Correspondence: andrea.a.perreault@vanderbilt.edu (A.A.P.), bjventers@gmail.com (B.J.V.)

https://doi.org/10.1016/j.isci.2020.101583

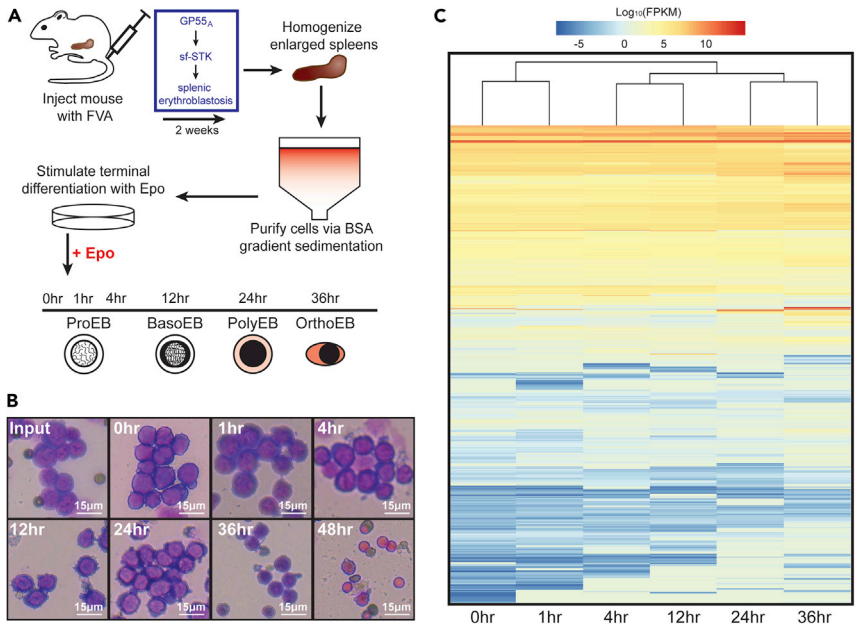

Figure 1. The FVA Murine System Faithfully Recapitulates Erythroid Differentiation during Erythropoiesis

(A) The workflow for generating and isolating highly purified EPO-responsive ProEBs from a mouse injected with the Friend virus that induces anemia (FVA).

(B) Microscopy images highlighting morphological changes of ProEBs isolated using the FVA system during differentiation.

(C) Heatmap of RNA-seq gene expression through erythroid differentiation.

Other TFs, such as YY1, are specifically enriched at chromatin loops that connect enhancers to promoters of actively transcribed genes (Weintraub et al., 2017). YY1 is a ubiquitously expressed zinc-finger TF that plays an important role in cellular differentiation (Kleiman et al., 2016; Beagan et al., 2017). Deletion of YY1-binding motifs at gene promoters in mouse embryonic stem cells (ESCs) reduced contact frequency between individual promoters and enhancers, and variably reduced mRNA levels (Weintraub et al., 2017). These data provide evidence for an essential role of YY1 in controlling gene expression by facilitating enhancer-promoter (E-P) interactions.

Erythropoiesis has been a useful model system for understanding the interplay between Pol II dynamics (Johnson et al., 2002; Sawado et al., 2003), enhancer activity (Reik et al., 1998), and 3D genome structure (Tolhuis et al., 2002; Chien et al., 2011; Deng et al., 2012; Bartman et al., 2016) during cellular differentiation. Indeed, we have previously characterized the genome-wide enhancer landscape in proerythroblasts (ProEBs) in response to erythropoietin (EPO) (Perreault et al., 2017), the hormone that is required for terminal erythroid differentiation (Koury and Bondurant, 1988, 1990). However, the manner by which EPO signaling shapes the 3D genome and specific chromatin interactions remains poorly understood. In addition, although CTCF occupancy and function has been assessed in erythroid cells (Hanssen et al., 2017; Hsu et al., 2017; Lee et al., 2017), the YY1-binding locations in erythroid cells are not known, resulting in a knowledge gap in uncovering the role of important TFs controlling E-P interactions and overall chromatin architecture during erythropoiesis.

To address this critical gap in understanding, we leveraged a murine model system to study synchronous erythroid maturation *ex vivo* in response to EPO stimulation (Figure 1) (Bondurant et al., 1985; Koury et al., 1984; Sawyer et al., 1987). Here, we demonstrate that EPO stimulates rapid transcriptional changes in ProEBs after 1 h (Figure 2). During this time, YY1 occupancy is dynamically redistributed, as opposed to CTCF, which remains unchanged (Figure 3). Moreover, there is little overlap in the regions bound by these structural TFs. Using HiChIP, we determined the chromatin contacts mediated by H3K27ac and YY1 genome-wide. We discover that a subset of these chromatin interactions remains invariant during EPO signaling, facilitating unique E-P interactions during EPO-mediated transcriptional regulation (Figure 4).

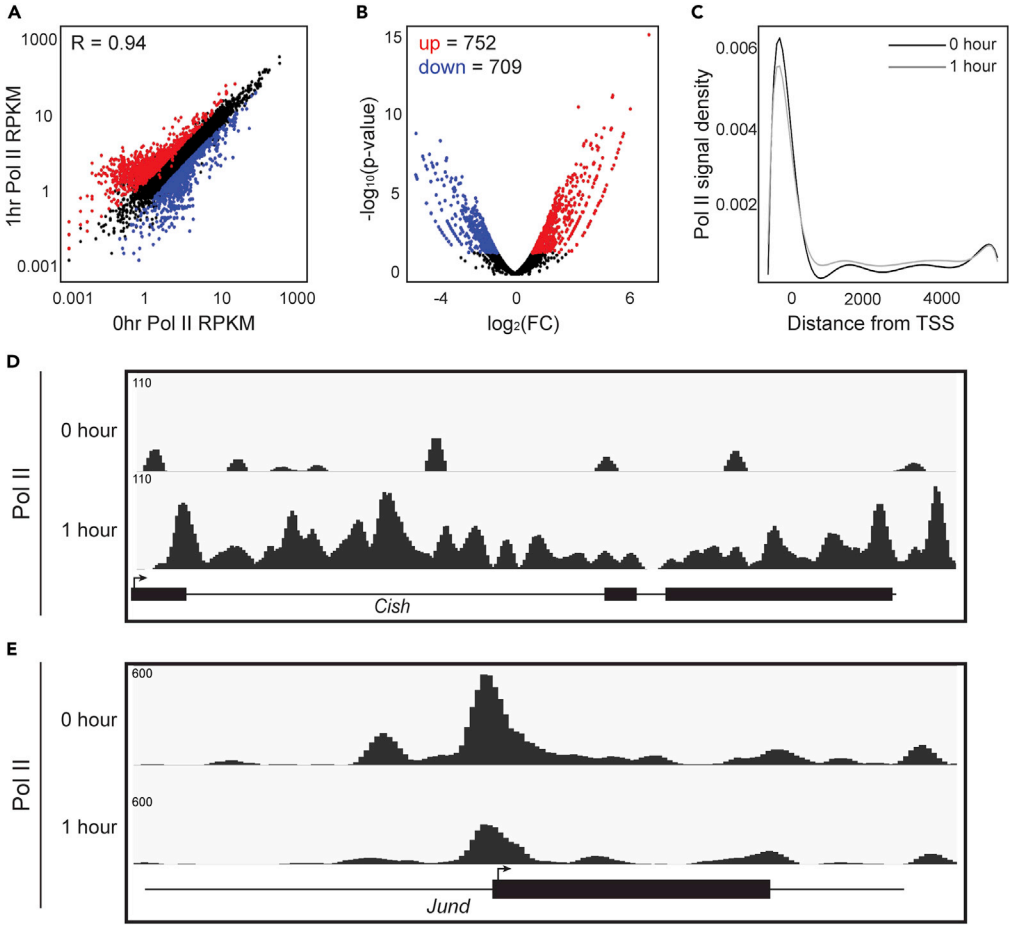

Figure 2. EPO Stimulation Results in Acute Transcriptional Changes in Proerythroblasts

(A) Scatterplot comparing Pol II RPKM before and after 1 h EPO stimulation. Pearson's correlation value R = 0.94.

(B) Volcano plot showing significant (p value < 0.05) differential occupancy of increased (red) and decreased (blue) Pol II after 1-h EPO stimulation.

(C–E) (C) Metagene plot comparing the position of Pol II peaks relative to transcription start site (TSS) (paired Wilcoxon ranked-sign test, $p = 4.882 \times 10^{-11}$). Genome browser view of ChIP-exo signal for Pol II at the up-regulated *Cish* locus (D) and down-regulated *Jund* locus (E).

RESULTS

EPO Induces Terminal Erythrocyte Differentiation through Changes in Gene Expression

The anemia-inducing strain of the Friend virus (FVA) system enables us to investigate the temporal dynamics of gene regulation and genome architecture in response to hormone stimulation. In this model, systemic treatment of mice with FVA induces ProEB proliferation in the spleen. After 14 days, large quantities of lineage-committed ProEBs can be isolated and purified. Stimulation of ProEBs with the hormone EPO in an *ex vivo* culture system induces synchronous terminal differentiation into mature erythrocytes over a 48 h period (Figure 1A) (Sawyer et al., 1987).

Using this model system, we observed a predictable shift in size and shape of maturing erythroid precursors during erythropoiesis, as visualized by light microscopy of H&E-stained cells. Before purification, the cells appear heterogeneous (Figure 1B, Input). After purification, a uniform population of ProEBs is obtained, evident as large, round cells. This morphological stage persists until approximately 12 h after the start of EPO stimulation (Figure 1B). After 24 h of EPO, cells form polychromatic erythroblasts (PolyEBs), characterized by the accumulation of hemoglobin, which coincides with the continued increase in globin gene expression. Finally, after 48 h of *ex vivo* culture in EPO, the cells have terminally differentiated into reticulocytes, marked by high hemoglobin production and nucleus extrusion (Figure 1B, 48hr).

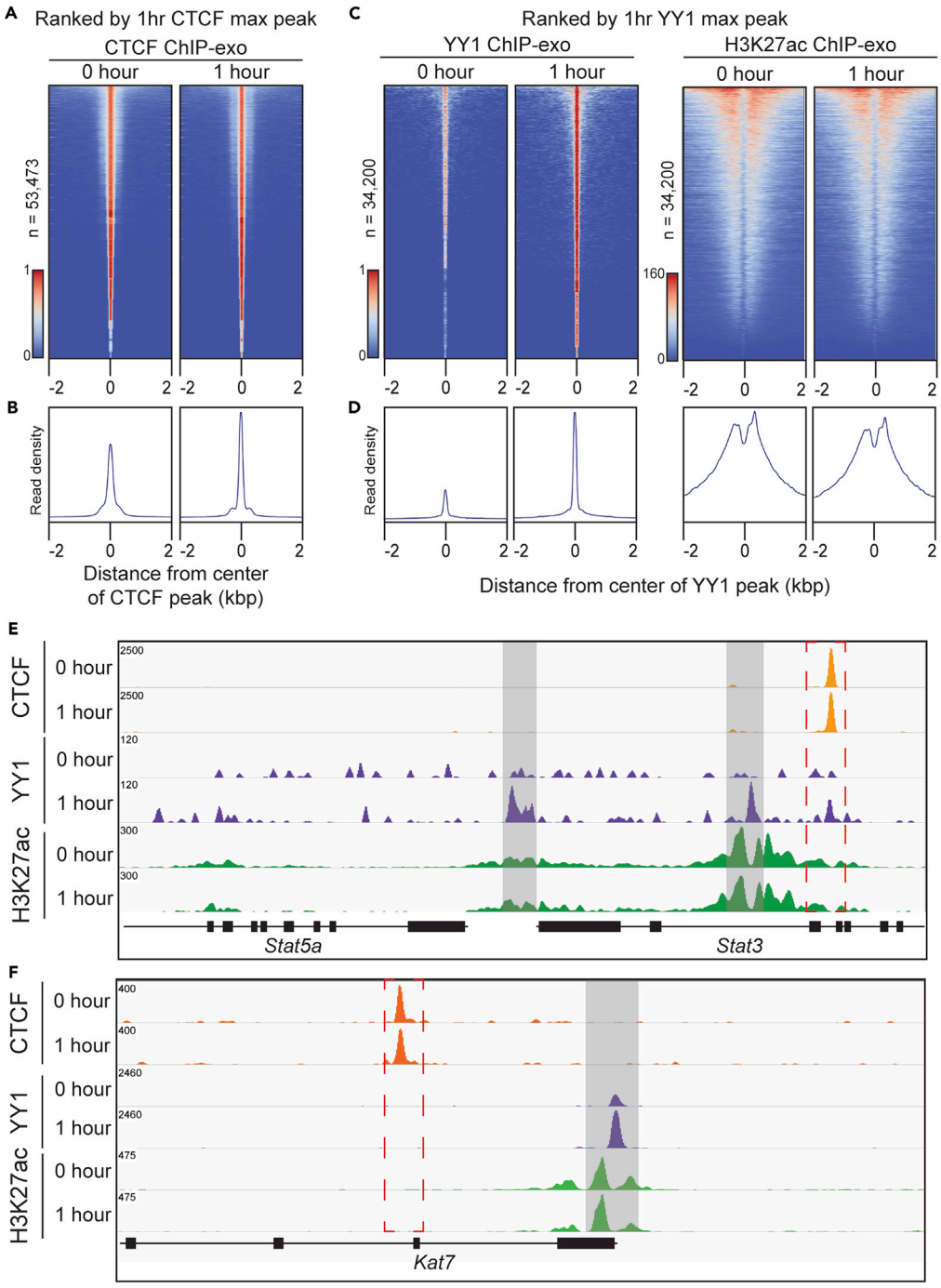

Figure 3. EPO Dynamically Regulates YY1 Occupancy Genome-wide

(A) Heatmap of CTCF peaks pre- and post-EPO stimulation, ranked by 1 h CTCF max peak.

(C) Heatmap of YY1 and H3K27ac peaks pre- and post-EPO stimulation, ranked by 1 h YY1 max peak.

(B and D) Composite plots below each heatmap quantifying the normalized tag density.

(E and F) Representative genome browser view of CTCF, YY1, and H3K27ac occupancy in response to EPO stimulation, highlighted in light gray bars and red dashed box.

Having established the kinetics of this model system, we next examined how differentiation impacts the erythroid gene expression program over time. RNA sequencing (RNA-seq) at six time points demonstrated both up- and down-regulation of genes when compared with EPO-naive cells (Figure 1C, Table S1).

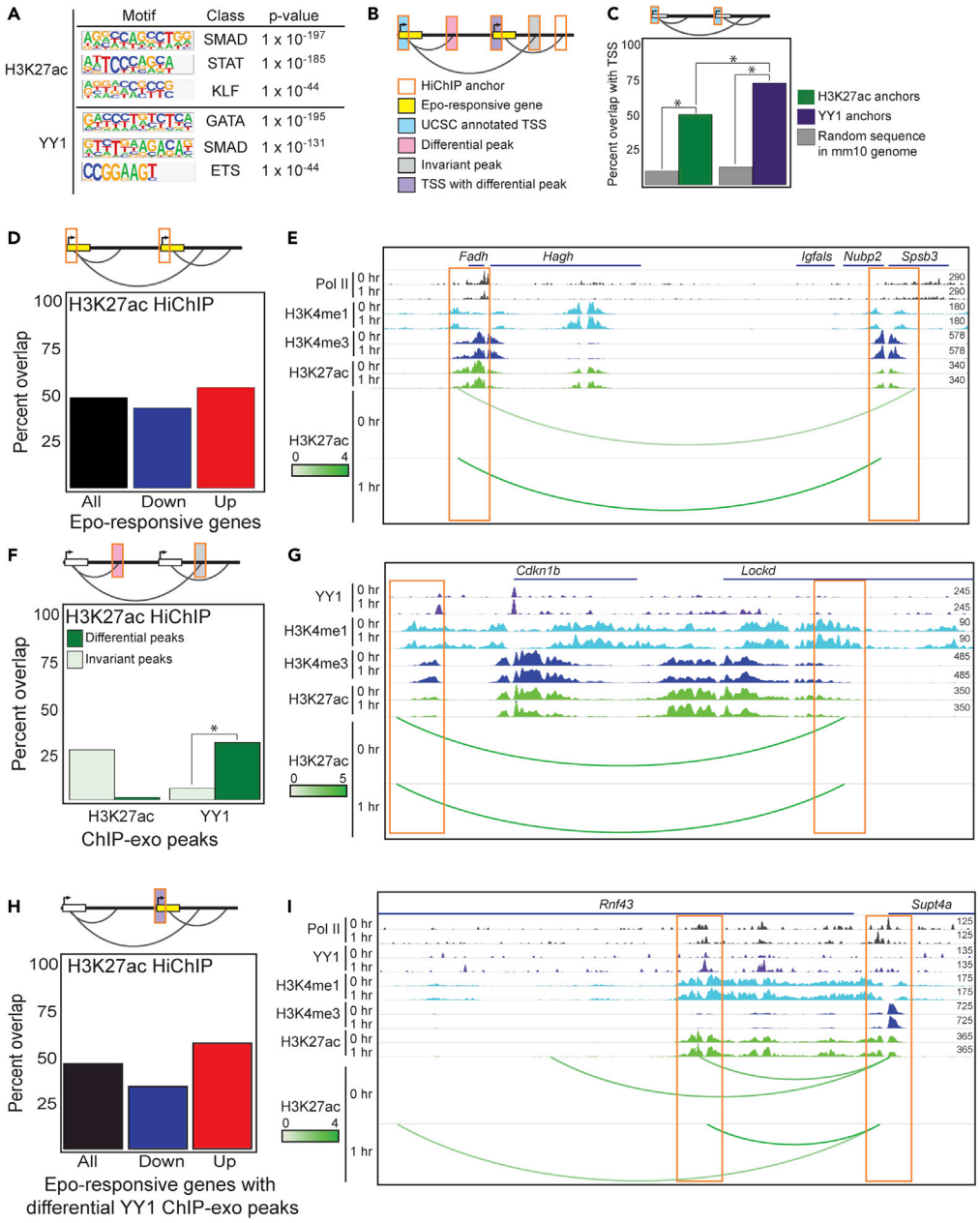

Figure 4. EPO Regulates Transcription in a Pre-established Chromatin Conformation

(A) TF-binding motifs overrepresented in HiChIP loop anchors.

(B) A schematic of chromatin features.

(C) Proportion of HiChIP interactions with UCSC-annotated TSS within anchor regions compared with random sequences in mm10 genome (gray bars) (*p < 0.0001). The hypergeometric test was applied to compare HiChIP anchors found in annotated TSSs to expected ratios. The chi-squared test was applied to compare TSS occupancy between H3K27ac and YY1 anchors, as well as comparing HiChIP anchors to randomly generated sequences in the mouse genome.

(D) Proportion of HiChIP interactions with promoters of EPO-responsive genes within H3K27ac HiChIP anchor regions.

(E) Representative genome browser view of overlap described in (D) with anchor regions highlighted in orange boxes.

(F) Proportion of HiChIP interactions with differential H3K27ac or YY1 ChIP-exo peaks within H3K27ac HiChIP anchor regions. Dark green bars represent differential peaks, and light green bars represent invariant peaks (*p < 0.0001). The chi-squared test was applied to compare YY1 differential and invariant peaks in H3K27ac anchors.

Figure 4. *Continued*

(G) Representative genome browser view of overlap described in (F) with anchor regions highlighted in orange boxes.
(H) Proportion of HiChIP interactions with differential YY1 peaks at promoters of EPO-responsive genes within H3K27ac HiChIP anchor regions.
(I) Representative genome browser view of overlap described in (H) with anchor regions highlighted in orange boxes.

Overall, approximately 12,000 genes had differential expression during the entire 48 h time course of erythropoiesis, with 8,105 of those genes significantly differentially expressed (adjusted q-value < 0.05). More specifically, there were 685 genes that significantly changed expression after only 1 h of EPO (adjusted q-value < 0.05). This transcriptomic dataset highlights the large changes in gene expression that accompany the morphological shifts occurring during erythropoiesis.

EPO Activates Rapid Transcriptional Changes in ProEBs

The progressive changes in gene expression observed by RNA-seq reflect global transcriptional responses. We set out to investigate the immediate transcriptional response to EPO in purified ProEBs. To assess the acute effect of hormone stimulation on transcription, we performed chromatin immunoprecipitation (ChIP)-exo for RNA polymerase II (Pol II) before and after 1 h of EPO stimulation. Overall, Pol II occupancy is highly correlated when comparing ChIP-exo signal pre- and post-EPO stimulation in this short time frame (Figure 2A, Table S2). This result indicates that global Pol II occupancy does not change at the majority of transcribed genes after 1 h. However, analysis of fold change of Pol II signal in these conditions did identify significant differential occupancy of Pol II at a smaller subset of genes ($p < 0.05$) (Figure 2B). We detected both significantly increased (n = 752, red) and decreased (n = 709, blue) Pol II signal at these EPO-responsive loci, indicating a set of genes that are regulated at the transcriptional level by EPO after only 1 h.

Overall, gene expression as measured by RNA-seq and transcription as measured by Pol II ChIP-exo are not in concordance with one another, specifically when investigating after 1 h EPO stimulation. There are 450 unique differentially expressed genes with consistent Pol II occupancy at promoters. Gene ontology (GO) analysis of these genes reveals an enrichment for genes involved in regulation of erythrocyte development, tyrosine phosphorylation of STAT protein, and response to hormonal stimulus, among others. This supports the role of the identified differentially expressed genes in response to EPO during erythroid maturation. However, when investigating stably expressed genes that have differential Pol II occupancy at promoters, there is no significant enrichment for specific biological processes. The explanation of the discordance of these features represents an area of gene regulation that requires further investigation.

Rapid transcriptional induction may reflect PIC assembly, pause release of Pol II, or a combination of these steps. To investigate the mechanism of EPO-regulated transcription, we next mapped Pol II signal at transcriptional start sites (TSS) or gene bodies of all induced genes. This approach identified that Pol II is more abundant at the TSS of genes before EPO (Figure 2C). After 1 h of EPO stimulation, Pol II transitions beyond the TSS into the gene body, indicative of pause release of Pol II at induced genes.

The dynamics of increased Pol II occupancy can be visualized at an exemplary locus of cytokine-inducible SH2-containing protein (*Cish*) (Figure 2D). *Cish* is a known target of the JAK-STAT signaling pathway, which is directly activated by EPO (Matsumoto et al., 1997; Rascle and Lees, 2003). We also observed down-regulation of transcription, including the *Jund* gene (Figure 2E). *Jund* is a component of the AP1 complex, which regulates response to cytokines, growth factors, stress, and infections in a variety of cellular contexts (Karin et al., 1997; Hernandez et al., 2008). *Jund*, along with other members of the Jun family, has been found to prevent differentiation in murine erythroleukemic cells (Prochownik et al., 1990), highlighting the critical need to down-regulate this gene during erythropoiesis. The importance of *Cish* and *Jund* in differentiation provides specific examples of the biological significance of the early EPO-mediated transcriptional responses described here.

EPO Dynamically Regulates YY1 Occupancy Genome-wide

Signal-dependent activation of Pol II is accompanied by alterations in chromatin organization. However, the impact of EPO on chromatin structure and function during erythropoiesis is not well understood. To begin addressing this question, we first examined the genome-wide occupancy patterns of CTCF and YY1, two TFs known to play key roles in genome organization and gene regulation. CTCF occupancy did not change between pre and post 1 h EPO treatment, as demonstrated by the comparison of global

enrichment analysis at each time point (Figures 3A and 3B, Tables S2 and S3). The stable CTCF-binding reflects the fact that the cells in each treatment group are lineage-committed ProEBs (Figures 1A and 1B). Thus, the invariant occupancy of CTCF observed is consistent with recent studies demonstrating that CTCF decreases variability in gene expression and thereby functions to maintain an established cell state (Ren et al., 2017).

In contrast to CTCF, YY1 is rapidly redistributed in the genome following 1 h EPO stimulation (Figures 3C and 3D, Tables S2 and S3). Of the 103,705 YY1 peaks found pre-EPO stimulation, only 4,843 peaks were found at the same regions after EPO stimulation. In EPO-naive ProEBs, the majority of YY1 localized to intergenic regions (blue region, 48%, Figure S1A). However, this localization shifted to intronic sites after EPO (gray region, 42%, Figure S1A). Notably, YY1 ChIP-exo signal at TSSs significantly increased from 5% to 17% following EPO (Figure S1A, hypergeometric test: p value <0.0001). These results specifically elaborate on the shifting genomic regions that YY1 binds pre and post 1 h of EPO stimulation. Comparison of CTCF and YY1 also revealed minimal overlap in localization of these two factors pre- and post-EPO stimulation, 7% and 5%, respectively (Figure S1B, hypergeometric test: p value < 0.0001). These results suggest that the chromatin domains established by CTCF and YY1 are distinct and these structural proteins have unique functions during EPO-dependent gene regulation in ProEBs.

In addition, ranking of H3K27ac signal by YY1 enrichment demonstrated that H3K27ac signal did not change in an appreciable manner compared with YY1 after EPO. This suggests that a subset of YY1 sites were more dynamic than H3K27ac, which is commonly used to identify active enhancers in the genome (Figures 3C and 3D).

At the *Stat3* gene, an exemplary locus of EPO-mediated transcription, a strong CTCF peak is evident pre-EPO and does not change after EPO (Figure 3E). At the same *Stat3* locus, YY1 occupancy increases at multiple *de novo* binding sites, as well as one site that overlaps with CTCF. Similar changes in YY1 can be visualized at another EPO-responsive gene, *Kat7* (Figure 3F). These specific loci illustrate how EPO induces a dynamic change in YY1 occupancy at a subset of genes relevant to signal transduction and chromatin modification during erythropoiesis.

EPO Regulates Transcription in a Pre-established Chromatin Conformation

Our discovery that YY1 rapidly redistributes in the ProEB genome following EPO stimulation prompted us to explore the role of YY1 and H3K27ac in chromatin organization. To accomplish this goal, we identified chromatin interactions using HiChIP (Table S4). HiChIP is a chromosome conformation capture assay that maps chromatin interactions between specific factors genome-wide (Mumbach et al., 2016). Chromatin interactions and high likelihood chromatin loops were identified using hichipper program (Tables S5 and S6) (for details, see Transparent Methods) (Lareau and Aryee, 2018b). We examined the global chromatin interactions mediated by YY1 or H3K27ac in EPO-stimulated ProEBs using Juicer (Durand et al., 2016) (Figures S2A–S2L). H3K27ac and YY1 anchors were approximately 4 kilobases (kb) on average both before and after EPO (Figure S3A). In addition, the average interaction lengths between either H3K27ac or YY1 anchors were approximately 317 kb, with no evident change in loop length in response to EPO treatment (Figure S3B).

To investigate the biological significance of these interactions in ProEBs, we first conducted unbiased, *de novo* motif discovery analysis using DNA sequences from all HiChIP anchor regions. Strikingly, we identified an enrichment of consensus motifs of multiple TF families known to regulate specification of the erythroid lineage, including STAT (Kisseleva et al., 2002; Watowich, 2011), KLF (Miller and Bieker, 1993; Cantor and Orkin, 2002; Kang et al., 2015), and GATA (Weiss and Orkin, 1995; Cantor and Orkin, 2002; Lentjes et al., 2016) (Figure 4A). In addition, auxiliary factors, such as SMAD and ETS, aid in the maintenance of gene expression and lineage commitment, respectively (Schmerer and Evans, 2003; Pimkin et al., 2014; Schuetze et al., 1993). The enrichment of these consensus motifs within YY1 and H3K27ac HiChIP anchor regions suggests functional coupling between erythroid TFs and chromatin conformation during erythropoiesis.

Overall, we identified 151,468 H3K27ac- and 138,583 YY1-mediated chromatin contacts in ProEBs using diffloop (for details, see Transparent Methods) (Lareau and Aryee, 2018a). The majority of these loops had a score less than 5 (Figures S3C and S3D), indicating that weak interactions predominate pre- and post-EPO

stimulation. Using fold change of loop scores as a metric for altered chromatin organization, we classified interactions as variant or invariant. We identified 109,390 invariant H3K27ac-mediated and 5,414 invariant YY1-mediated contacts. Interestingly, 99% of H3K27ac and 97% of YY1 strong contacts were invariant.

As strong contacts are likely to be more robust than other contacts, we therefore focused further investigation on invariant loops to gain insight into the relationship between constant chromatin organization and transcriptional response, as has been conducted in recent literature (Jin et al., 2013; D'Ippolito et al., 2018; Ray et al., 2019). We reasoned that a better understanding of the interactions between enhancers and promoters might provide new insights into how EPO regulates transcription. We classified 23,423 H3K27ac and 21,777 YY1 E-P loops using diffloop (Lareau and Aryee, 2018a), which were further delineated into 16,698 and 1,444 invariant E-P loops for H3K27ac and YY1, respectively. The majority of E-P loops are found in intronic regions and did not shift location in the genome based on variance or factor (Figure S3E).

To gain insights into how E-P loops are involved in transcriptional regulation, we aimed to investigate the interplay of chromatin interactions, gene expression, and TF binding. The schematic in Figure 4B depicts these features.

We first quantified the proportion of HiChIP anchors (H3K27ac or YY1) of invariant E-P contacts that map to UCSC-annotated TSSs in the mm10 reference genome (Figure 4C). We would expect 50% of the anchors to be found in TSS regions if each promoter was connected to one enhancer. Indeed, 50% of the H3K27ac anchors were observed in annotated TSSs (Figure 4C, hypergeometric test: $p < 0.0001$). In contrast to H3K27ac, 73% of YY1 anchors overlapped with annotated TSSs, indicating that more YY1 anchors are at promoters compared with enhancer regions (Figure 4C, hypergeometric test: $p < 0.0001$). These results suggest that a single enhancer could regulate the transcription of multiple target genes in chromatin interactions mediated by YY1. The difference in TSS occupancy between H3K27ac and YY1 anchors is significant (chi-squared: $p < 0.0001$), indicating that H3K27ac and YY1 are differentially mediating E-P interactions and their connectivity. As an additional validation, we randomly generated sequences of the mouse genome and overlapped these with anchor regions (gray bars, Figure 4C, chi-squared: $p < 0.00001$), which supports the conclusion that annotated TSSs are more likely to be found at loop anchors than expected due to chance.

Given that E-P interactions overlap with annotated promoter regions, we next examined the relationship between these contacts and the associated changes in transcriptional response to EPO, as described in Figure 2. Focusing only on EPO-responsive genes (n = 1,462), we identified a higher proportion of overlap for H3K27ac anchors at promoters of EPO-responsive genes when compared with YY1 anchors, 50% (Figure 4D) and 6% (Figure S4A), respectively. We also examined this relationship as a function of genes up- (n = 752, red) or down-regulated (n = 709, blue) by EPO. As expected, fewer promoters in EPO down-regulated genes overlapped with H3K27ac anchors. The persistence of H3K27ac in down-regulated promoters is consistent with prior work demonstrating that loss of H3K27ac signal at enhancers and promoters can lag behind a decrease in transcription (Brown et al., 2014). The majority (75%) of strong H3K27ac loops, however, were found at genes that were not responsive to EPO, suggesting that strong, invariant interactions sustain transcription during response to external stimulation. Figure 4E shows a representative example of this overlap at the *Fadh1* gene, which is intricately involved in mitochondrial activity and metabolism (Weiss et al., 2018). Mitochondrial biogenesis is activated by EPO and is therefore highly regulated during erythropoiesis (Carraway et al., 2010; Liu et al., 2017). These data reveal that H3K27ac-mediated loops that are weak or moderate in strength are connected to EPO-induced transcriptional response.

We were surprised that H3K27ac anchors overlapped at promoters of EPO-responsive genes more than YY1 anchors, given that YY1 genome occupancy was more dynamic (Figure 3). To resolve this apparent paradox, we first examined the relationship between differential H3K27ac or YY1 occupancy and invariant chromatin contacts. With this approach, we detected significant enrichment for differential YY1 ChIP-exo peaks at invariant H3K27ac anchors (Figure 4F, chi-squared: $p < 0.0001$). In contrast to this result, invariant H3K27ac loops were associated with invariant H3K27ac ChIP-exo peaks (Figure 4F). An example of this relationship can be observed at the *Cdkn1b and Lockd* loci, two genes that regulate exit of erythroid precursors from the cell cycle, a required step in differentiation

(Paralkar et al., 2016) (Figure 4G). Similarly, anchors of invariant YY1 chromatin interactions were enriched at loci with differential YY1 and invariant H3K27ac ChIP-exo peaks (Figure S4B). This suggests that although certain factors, like YY1, are more dynamic than others, like H3K27ac, these features do not necessarily indicate the variance of the loops they mediate.

We then wanted to test if YY1 differential occupancy at promoters was related to transcriptional response to EPO. Indeed, this analysis revealed that H3K27ac anchors were found at promoters of EPO-responsive genes with differential YY1 ChIP-exo peaks (Figure 4H). This supports the idea that invariant chromatin interactions are facilitative environments for transcriptional and epigenetic response to hormone stimulation. A representative example of this overlap is shown at the *Supt4a* gene, which encodes the SPT4 protein, a component of the DSIF elongation complex (Schneider et al., 2006; Crickard et al., 2017), implicating this locus in transcriptional regulation. By contrast, YY1 anchors were not enriched for differential YY1 peaks or EPO-responsive genes to the same degree as H3K27ac anchors (Figure S4C). This suggests that H3K27ac and YY1 regulate chromatin architecture and therefore gene regulation through different mechanisms. Together, these results support a model whereby EPO induces dynamic transcription and TF binding within a pre-established chromatin context.

DISCUSSION

The findings presented here examining erythroid differentiation in response to EPO are consistent with an emerging paradigm that signal-dependent transcriptional responses occur within a pre-established chromatin landscape identified using HiC methodologies. For example, TNFalpha-responsive enhancers in human fibroblasts were already in contact with their target promoters before signaling. These results suggest a model in which signal-responsive TFs bind to enhancers to function within a pre-established chromatin architecture (Jin et al., 2013). Glucocorticoid treatment in human A549 cells revealed that glucocorticoid receptor binding to the genome did not promote new chromatin contacts, but instead induced changes in existing interactions to regulate transcription (D'Ippolito et al., 2018). HiC analysis in *Drosophila* S2 and human K562 cells identified that no global changes in TADs emerged after heat shock treatment, despite changes in TF binding and induction of heat shock response genes (Ray et al., 2019). Finally, capture HiC and 4C experiments in ESCs have provided evidence that hardwired chromatin interactions provide an environment for TF binding and enhancer activation that facilitates a rapid transcriptional response to signaling in neuronal development (Atlasi et al., 2019). Unlike these studies, our study employed the HiChIP assay to define the genome-wide contacts mediated by specific factors, namely, H3K27ac and YY1. These H3K27ac and YY1 HiChIP contacts revealed a subset of invariant chromatin loops that connect enhancers and EPO-regulated genes, thereby refining the E-P connectome in erythroid cells. These chromatin interactions provide important insights to conformational features, such as enhancer skipping and promoter-promoter interactions, which cannot be determined using 1D chromatin features (Mumbach et al., 2017). Future work will investigate these conformation features to evaluate previously identified E-P interactions in ProEBs (Perreault et al., 2017).

Given that CTCF domains shift during development (Nora et al., 2017), we originally hypothesized that EPO would induce changes to CTCF occupancy and subTAD organization. However, CTCF occupancy did not change but instead decreased after EPO, supporting the idea of selective pruning of CTCF-binding sites during differentiation (Beagan et al., 2017). In contrast, YY1 did redistribute dynamically in the genome within 1 h of EPO stimulation, suggesting a more critical role for YY1 in chromatin organization in early erythroid maturation. These data are consistent with studies identifying YY1's role in E-P loops and transcriptional activation (Weintraub et al., 2017). Given that YY1 was more dynamic than H3K27ac occupancy, we speculate that combining H3K27ac and YY1 occupancy data may assign enhancers to target genes with more accuracy than H3K27ac alone. This concept will require additional studies.

Not surprisingly, we did observe dynamic changes in Pol II occupancy in response to EPO at a subset of genes both significantly up- and down-regulated. These results are consistent with a growing body of work identifying paused Pol II at signal-responsive genes. It has been proposed that this state of Pol II enables rapid transcriptional response to environmental stimuli. For example, in *Drosophila* S2 cells stalled Pol II was strongly enriched at genes that are induced by multiple signaling pathways involved in regulating development, cell differentiation, and cell communication (Muse et al., 2007). In addition, study of murine macrophage cell lines identified an accumulation of paused Pol II at the *TNFalpha* gene in quiescent cells before induction of the gene by inflammatory cytokines (Adelman et al., 2009).

There are still several aspects of EPO's impact on transcription and chromatin structure that remain unanswered. We identified discordance between dynamic YY1 binding measured by ChIP-exo and invariant YY1-mediated interactions determined by HiChIP. The majority of YY1 HiChIP interactions had weak scores (scores <5, Figure S3D), despite abundant YY1 binding in the genome. This suggests that the overall abundance of YY1 does not necessarily indicate the strength of the loop it mediates. It is possible that YY1-binding locations are establishing chromatin contacts that will gain strength over time, and therefore delineate cell-type-specific interactions more decisively as maturation continues. In addition, we expected Pol II ChIP-exo differential peaks to be found at gene promoters that exhibited differential expression as measured by RNA-seq. However, we only detected a small overlap in the gene promoters where this was the case. It is likely that steady-state gene expression measured by RNA-seq lags behind rapid transcriptional responses assessed by Pol II ChIP-exo. Future studies will investigate this relationship between Pol II occupancy and gene expression across the entire period of erythroid maturation in the FVA model.

Taken together, the results presented here integrate epigenetic and transcriptional profiles with genome-wide HiChIP datasets to describe how hormone stimulation regulates erythroid differentiation. We demonstrate that dynamic features occur within static chromatin interactions. Future work will focus on integrating changes in Pol II, CTCF, H3K27ac, and YY1, as well as the chromatin contacts they mediate, during erythropoiesis with the goal of understanding how the 3D genome influences transcription and dynamic gene regulatory programs during erythroid maturation. This knowledge will have a significant impact on our understanding of the interplay between signal-dependent transcription and chromatin architecture.

Limitations of the Study

Although the FVA system provides the ideal model system to study isolated, pure populations of cells during erythroid differentiation, the presented study investigates the first hour of erythropoiesis. There are transcriptional and epigenetic dynamics during this narrow time frame, but the large-scale changes that occur during erythroid maturation remain to be investigated. Mainly, the invariant chromatin structure described here may be a unique feature of the ProEBs that have been stimulated with EPO for 1 h. In addition, the discordance of gene expression as measured by RNA-seq and the transcriptional responses assessed by Pol II ChIP-exo may be a result of the short stimulation time studied here.

Resource Availability

Lead Contact

Further information and requests for resources and reagents should be directed to and will be fulfilled by the Lead Contact, Andrea Perreault (andrea.a.perreault@vanderbilt.edu).

Materials Availability

This study did not generate new unique reagents.

Data and Code Availability

Unpublished custom code is available upon request from the Lead Contact. Summary of sequencing statistics can be found in Tables S1, S2, and S4. The accession number for the data reported in this paper is GEO SuperSeries GEO: GSE142006. Individual datasets can be found at GEO: GSE142003 (ChIP), GEO: GSE142004 (HiChIP), and GEO: GSE142005 (RNA-seq).

METHODS

All methods can be found in the accompanying Transparent Methods supplemental file.

SUPPLEMENTAL INFORMATION

Supplemental Information can be found online at https://doi.org/10.1016/j.isci.2020.101583.

ACKNOWLEDGMENTS

A.A.P. was supported by the Vanderbilt Molecular Endocrinology Training Program (NIDDK, grant 5T32 DK07563). We would like to thank the Vanderbilt Technologies for Advanced Genomics (VANTAGE) Core for technical support with Illumina sequencing and Vanderbilt Technologies for Advanced Genomics Analysis and Research Design (VANGUARD) Core for guidance on statistical analysis. Special thanks also

go to Nicholas Servant, Maxwell Mumbach, and Caleb Lareau for experimental and computational assistance.

AUTHOR CONTRIBUTIONS

Conceptualization, A.A.P. and B.J.V.; Methodology, A.A.P. and B.J.V.; Formal Analysis, A.A.P.; Investigation, A.A.P.; Resources, A.A.P.; Writing – Original Draft, A.A.P.; Writing – Review and Editing, A.A.P., J.D.B., and B.J.V.; Supervision, J.D.B. and B.J.V.

DECLARATION OF INTERESTS

The authors declare no competing interests.

Received: May 1, 2020
Revised: August 7, 2020
Accepted: September 16, 2020
Published: October 23, 2020

REFERENCES

Adelman, K., Kennedy, M.A., Nechaev, S., Gilchrist, D.A., Muse, G.W., Chinenov, Y., and Rogatsky, I. (2009). Immediate mediators of the inflammatory response are poised for gene activation through RNA polymerase II stalling. Proc. Natl. Acad. Sci. U S A *106*, 18207–18212.

Arzate-Mejia, R.G., Recillas-Targa, F., and Corces, V.G. (2018). Developing in 3D: the role of CTCF in cell differentiation. Development *145*, dev137729.

Atlasi, Y., Megchelenbrink, W., Peng, T., Habibi, E., Joshi, O., Wang, S.Y., Wang, C., Logie, C., Poser, I., Marks, H., and Stunnenberg, H.G. (2019). Epigenetic modulation of a hardwired 3D chromatin landscape in two naive states of pluripotency. Nat. Cell Biol. *21*, 568–578.

Bartman, C.R., Hsu, S.C., Hsiung, C.C., Raj, A., and Blobel, G.A. (2016). Enhancer regulation of transcriptional bursting parameters revealed by forced chromatin looping. Mol. Cell *62*, 237–247.

Beagan, J.A., Duong, M.T., Titus, K.R., Zhou, L., Cao, Z., Ma, J., Lachanski, C.V., Gillis, D.R., and Phillips-Cremins, J.E. (2017). YY1 and CTCF orchestrate a 3D chromatin looping switch during early neural lineage commitment. Genome Res. *27*, 1139–1152.

Bondurant, M.C., Lind, R.N., Koury, M.J., and Ferguson, M.E. (1985). Control of globin gene transcription by erythropoietin in erythroblasts from friend virus-infected mice. Mol. Cell Biol. *5*, 675–683.

Brown, J.D., Lin, C.Y., Duan, Q., Griffin, G., Federation, A., Paranal, R.M., Bair, S., Newton, G., Lichtman, A., Kung, A., et al. (2014). NF-kappaB directs dynamic super enhancer formation in inflammation and atherogenesis. Mol. Cell *56*, 219–231.

Cantor, A.B., and Orkin, S.H. (2002). Transcriptional regulation of erythropoiesis: an affair involving multiple partners. Oncogene *21*, 3368–3376.

Carraway, M.S., Suliman, H.B., Jones, W.S., Chen, C.W., Babiker, A., and Piantadosi, C.A. (2010). Erythropoietin activates mitochondrial biogenesis and couples red cell mass to mitochondrial mass in the heart. Circ. Res. *106*, 1722–1730.

Chien, R., Zeng, W., Kawauchi, S., Bender, M.A., Santos, R., Gregson, H.C., Schmiesing, J.A., Newkirk, D.A., Kong, X., Ball, A.R., Jr., et al. (2011). Cohesin mediates chromatin interactions that regulate mammalian beta-globin expression. J. Biol. Chem. *286*, 17870–17878.

Crickard, J.B., Lee, J., Lee, T.H., and Reese, J.C. (2017). The elongation factor Spt4/5 regulates RNA polymerase II transcription through the nucleosome. Nucleic Acids Res. *45*, 6362–6374.

D'ippolito, A.M., Mcdowell, I.C., Barrera, A., Hong, L.K., Leichter, S.M., Bartelt, L.C., Vockley, C.M., Majoros, W.H., Safi, A., Song, L., et al. (2018). Pre-established chromatin interactions mediate the genomic response to glucocorticoids. Cell Syst. *7*, 146–160 e7.

Danko, C.G., Hah, N., Luo, X., Martins, A.L., Core, L., Lis, J.T., Siepel, A., and Kraus, W.L. (2013). Signaling pathways differentially affect RNA polymerase II initiation, pausing, and elongation rate in cells. Mol. Cell *50*, 212–222.

Deng, W., Lee, J., Wang, H., Miller, J., Reik, A., Gregory, P.D., Dean, A., and Blobel, G.A. (2012). Controlling long-range genomic interactions at a native locus by targeted tethering of a looping factor. Cell *149*, 1233–1244.

Dixon, J.R., Selvaraj, S., Yue, F., Kim, A., Li, Y., Shen, Y., Hu, M., Liu, J.S., and Ren, B. (2012). Topological domains in mammalian genomes identified by analysis of chromatin interactions. Nature *485*, 376–380.

Dowen, J.M., Fan, Z.P., Hnisz, D., Ren, G., Abraham, B.J., Zhang, L.N., Weintraub, A.S., Schujiers, J., Lee, T.I., Zhao, K., and Young, R.A. (2014). Control of cell identity genes occurs in insulated neighborhoods in mammalian chromosomes. Cell *159*, 374–387.

Durand, N.C., Shamim, M.S., Machol, I., Rao, S.S., Huntley, M.H., Lander, E.S., and Aiden, E.L. (2016). Juicer provides a one-click system for analyzing loop-resolution Hi-C experiments. Cell Syst. *3*, 95–98.

Ernst, J., Kheradpour, P., Mikkelsen, T.S., Shoresh, N., Ward, L.D., Epstein, C.B., Zhang, X., Wang, L., Issner, R., Coyne, M., et al. (2011). Mapping and analysis of chromatin state dynamics in nine human cell types. Nature *473*, 43–49.

Fullwood, M.J., Liu, M.H., Pan, Y.F., Liu, J., Xu, H., Mohamed, Y.B., Orlov, Y.L., Velkov, S., Ho, A., Mei, P.H., et al. (2009). An oestrogen-receptor-alpha-bound human chromatin interactome. Nature *462*, 58–64.

Gaertner, B., Johnston, J., Chen, K., Wallaschek, N., Paulson, A., Garruss, A.S., Gaudenz, K., De Kumar, B., Krumlauf, R., and Zeitlinger, J. (2012). Poised RNA polymerase II changes over developmental time and prepares genes for future expression. Cell Rep. *2*, 1670–1683.

Hanssen, L.L.P., Kassouf, M.T., Oudelaar, A.M., Biggs, D., Preece, C., Downes, D.J., Gosden, M., Sharpe, J.A., Sloane-Stanley, J.A., Hughes, J.R., et al. (2017). Tissue-specific CTCF-cohesin-mediated chromatin architecture delimits enhancer interactions and function in vivo. Nat. Cell Biol. *19*, 952–961.

Heintzman, N.D., Hon, G.C., Hawkins, R.D., Kheradpour, P., Stark, A., Harp, L.F., Ye, Z., Lee, L.K., Stuart, R.K., Ching, C.W., et al. (2009). Histone modifications at human enhancers reflect global cell-type-specific gene expression. Nature *459*, 108–112.

Hernandez, J.M., Floyd, D.H., Weilbaecher, K.N., Green, P.L., and Boris-Lawrie, K. (2008). Multiple facets of junD gene expression are atypical among AP-1 family members. Oncogene *27*, 4757–4767.

Hsu, S.C., Gilgenast, T.G., Bartman, C.R., Edwards, C.R., Stonestrom, A.J., Huang, P., Emerson, D.J., Evans, P., Werner, M.T., Keller, C.A., et al. (2017). The BET protein BRD2 cooperates with CTCF to enforce transcriptional and architectural boundaries. Mol. Cell *66*, 102–116.e7.

Ji, X., Dadon, D.B., Powell, B.E., Fan, Z.P., Borges-Rivera, D., Shachar, S., Weintraub, A.S., Hnisz, D., Pegoraro, G., Lee, T.I., et al. (2016). 3D

chromosome regulatory landscape of human pluripotent cells. Cell Stem Cell *18*, 262–275.

Jin, F., Li, Y., Dixon, J.R., Selvaraj, S., Ye, Z., Lee, A.Y., Yen, C.A., Schmitt, A.D., Espinoza, C.A., and Ren, B. (2013). A high-resolution map of the three-dimensional chromatin interactome in human cells. Nature *503*, 290–294.

Johnson, K.D., Grass, J.A., Boyer, M.E., Kiekhaefer, C.M., Blobel, G.A., Weiss, M.J., and Bresnick, E.H. (2002). Cooperative activities of hematopoietic regulators recruit RNA polymerase II to a tissue-specific chromatin domain. Proc. Natl. Acad. Sci. U S A *99*, 11760–11765.

Kang, Y., Kim, Y.W., Yun, J., Shin, J., and Kim, A. (2015). KLF1 stabilizes GATA-1 and TAL1 occupancy in the human beta-globin locus. Biochim. Biophys. Acta *1849*, 282–289.

Karin, M., Liu, Z., and Zandi, E. (1997). AP-1 function and regulation. Curr. Opin. Cell Biol. *9*, 240–246.

Kisseleva, T., Bhattacharya, S., Braunstein, J., and Schindler, C.W. (2002). Signaling through the JAK/STAT pathway, recent advances and future challenges. Gene *285*, 1–24.

Kleiman, E., Jia, H., Loguercio, S., Su, A.I., and Feeney, A.J. (2016). YY1 plays an essential role at all stages of B-cell differentiation. Proc. Natl. Acad. Sci. U S A *113*, E3911–E3920.

Koury, M.J., and Bondurant, M.C. (1988). Maintenance by erythropoietin of viability and maturation of murine erythroid precursor cells. J. Cell Physiol. *137*, 65–74.

Koury, M.J., and Bondurant, M.C. (1990). Erythropoietin retards DNA breakdown and prevents programmed death in erythroid progenitor cells. Science *248*, 378–381.

Koury, M.J., Sawyer, S.T., and Bondurant, M.C. (1984). Splenic erythroblasts in anemia-inducing Friend disease: a source of cells for studies of erythropoietin-mediated differentiation. J. Cell. Physiol. *121*, 526–532.

Lareau, C.A., and Aryee, M.J. (2018a). diffloop: a computational framework for identifying and analyzing differential DNA loops from sequencing data. Bioinformatics *34*, 672–674.

Lareau, C.A., and Aryee, M.J. (2018b). hichipper: a preprocessing pipeline for calling DNA loops from HiChIP data. Nat. Methods *15*, 155–156.

Lee, J., Krivega, I., Dale, R.K., and Dean, A. (2017). The LDB1 complex Co-opts CTCF for erythroid lineage-specific long-range enhancer interactions. Cell Rep. *19*, 2490–2502.

Lentjes, M.H., Niessen, H.E., Akiyama, Y., De Bruine, A.P., Melotte, V., and Van Engeland, M. (2016). The emerging role of GATA transcription factors in development and disease. Expert Rev. Mol. Med. *18*, e3.

Li, G., Ruan, X., Auerbach, R.K., Sandhu, K.S., Zheng, M., Wang, P., Poh, H.M., Goh, Y., Lim, J., Zhang, J., et al. (2012). Extensive promoter-centered chromatin interactions provide a topological basis for transcription regulation. Cell *148*, 84–98.

Lieberman-Aiden, E., Van Berkum, N.L., Williams, L., Imakaev, M., Ragoczy, T., Telling, A., Amit, I., Lajoie, B.R., Sabo, P.J., Dorschner, M.O., et al. (2009). Comprehensive mapping of long-range interactions reveals folding principles of the human genome. Science *326*, 289–293.

Liu, X., Kraus, W.L., and Bai, X. (2015). Ready, pause, go: regulation of RNA polymerase II pausing and release by cellular signaling pathways. Trends Biochem. Sci. *40*, 516–525.

Liu, X., Zhang, Y., Ni, M., Cao, H., Signer, R.A.J., Li, D., Li, M., Gu, Z., Hu, Z., Dickerson, K.E., et al. (2017). Regulation of mitochondrial biogenesis in erythropoiesis by mTORC1-mediated protein translation. Nat. Cell Biol. *19*, 626–638.

Matsumoto, A., Masuhara, M., Mitsui, K., Yokouchi, M., Ohtsubo, M., Misawa, H., Miyajima, A., and Yoshimura, A. (1997). CIS, a cytokine inducible SH2 protein, is a target of the JAK-STAT5 pathway and modulates STAT5 activation. Blood *89*, 3148–3154.

Miller, I.J., and Bieker, J.J. (1993). A novel, erythroid cell-specific murine transcription factor that binds to the CACCC element and is related to the Kruppel family of nuclear proteins. Mol. Cell Biol. *13*, 2776–2786.

Mora, A., Sandve, G.K., Gabrielsen, O.S., and Eskeland, R. (2016). In the loop: promoter-enhancer interactions and bioinformatics. Brief Bioinform. *17*, 980–995.

Mumbach, M.R., Rubin, A.J., Flynn, R.A., Dai, C., Khavari, P.A., Greenleaf, W.J., and Chang, H.Y. (2016). HiChIP: efficient and sensitive analysis of protein-directed genome architecture. Nat. Methods *13*, 919–922.

Mumbach, M.R., Satpathy, A.T., Boyle, E.A., Dai, C., Gowen, B.G., Cho, S.W., Nguyen, M.L., Rubin, A.J., Granja, J.M., Kazane, K.R., et al. (2017). Enhancer connectome in primary human cells identifies target genes of disease-associated DNA elements. Nat. Genet. *49*, 1602–1612.

Muse, G.W., Gilchrist, D.A., Nechaev, S., Shah, R., Parker, J.S., Grissom, S.F., Zeitlinger, J., and Adelman, K. (2007). RNA polymerase is poised for activation across the genome. Nat. Genet. *39*, 1507–1511.

Nora, E.P., Goloborodko, A., Valton, A.L., Gibcus, J.H., Uebersohn, A., Abdennur, N., Dekker, J., Mirny, L.A., and Bruneau, B.G. (2017). Targeted degradation of CTCF decouples local insulation of chromosome domains from genomic compartmentalization. Cell *169*, 930–944.e22.

Ong, C.T., and Corces, V.G. (2014). CTCF: an architectural protein bridging genome topology and function. Nat. Rev. Genet. *15*, 234–246.

Paralkar, V.R., Taborda, C.C., Huang, P., Yao, Y., Kossenkov, A.V., Prasad, R., Luan, J., Davies, J.O., Hughes, J.R., Hardison, R.C., et al. (2016). Unlinking an lncRNA from its associated cis element. Mol. Cell *62*, 104–110.

Perreault, A.A., Benton, M.L., Koury, M.J., Brandt, S.J., and Venters, B.J. (2017). Epo reprograms the epigenome of erythroid cells. Exp. Hematol. *51*, 47–62.

Phillips, J.E., and Corces, V.G. (2009). CTCF: master weaver of the genome. Cell *137*, 1194–1211.

Pimkin, M., Kossenkov, A.V., Mishra, T., Morrissey, C.S., Wu, W., Keller, C.A., Blobel, G.A., Lee, D., Beer, M.A., Hardison, R.C., and Weiss, M.J. (2014). Divergent functions of hematopoietic transcription factors in lineage priming and differentiation during erythro-megakaryopoiesis. Genome Res. *24*, 1932–1944.

Prochownik, E.V., Smith, M.J., Snyder, K., and Emeagwali, D. (1990). Amplified expression of three jun family members inhibits erythroleukemia differentiation. Blood *76*, 1830–1837.

Rao, S.S., Huntley, M.H., Durand, N.C., Stamenova, E.K., Bochkov, I.D., Robinson, J.T., Sanborn, A.L., Machol, I., Omer, A.D., Lander, E.S., and Aiden, E.L. (2014). A 3D map of the human genome at kilobase resolution reveals principles of chromatin looping. Cell *159*, 1665–1680.

Rao, S.S.P., Huang, S.C., Glenn St Hilaire, B., Engreitz, J.M., Perez, E.M., Kieffer-Kwon, K.R., Sanborn, A.L., Johnstone, S.E., Bascom, G.D., Bochkov, I.D., et al. (2017). Cohesin loss eliminates all loop domains. Cell *171*, 305–320 e24.

Rascle, A., and Lees, E. (2003). Chromatin acetylation and remodeling at the Cis promoter during STAT5-induced transcription. Nucleic Acids Res. *31*, 6882–6890.

Ray, J., Munn, P.R., Vihervaara, A., Lewis, J.J., Ozer, A., Danko, C.G., and Lis, J.T. (2019). Chromatin conformation remains stable upon extensive transcriptional changes driven by heat shock. Proc. Natl. Acad. Sci. U S A *116*, 19431–19439.

Reik, A., Telling, A., Zitnik, G., Cimbora, D., Epner, E., and Groudine, M. (1998). The locus control region is necessary for gene expression in the human beta-globin locus but not the maintenance of an open chromatin structure in erythroid cells. Mol. Cell Biol. *18*, 5992–6000.

Ren, G., Jin, W., Cui, K., Rodrigez, J., Hu, G., Zhang, Z., Larson, D.R., and Zhao, K. (2017). CTCF-mediated enhancer-promoter interaction is a critical regulator of cell-to-cell variation of gene expression. Mol. Cell *67*, 1049–1058 e6.

Sanyal, A., Lajoie, B.R., Jain, G., and Dekker, J. (2012). The long-range interaction landscape of gene promoters. Nature *489*, 109–113.

Sawado, T., Halow, J., Bender, M.A., and Groudine, M. (2003). The beta -globin locus control region (LCR) functions primarily by enhancing the transition from transcription initiation to elongation. Genes Dev. *17*, 1009–1018.

Sawyer, S.T., Koury, M.J., and Bondurant, M.C. (1987). Large-scale procurement of erythropoietin-responsive erythroid cells: assay

for biological activity of erythropoietin. Methods Enzymol. *147*, 340–352.

Schmerer, M., and Evans, T. (2003). Primitive erythropoiesis is regulated by Smad-dependent signaling in postgastrulation mesoderm. Blood *102*, 3196–3205.

Schneider, D.A., French, S.L., Osheim, Y.N., Bailey, A.O., Vu, L., Dodd, J., Yates, J.R., Beyer, A.L., and Nomura, M. (2006). RNA polymerase II elongation factors Spt4p and Spt5p play roles in transcription elongation by RNA polymerase I and rRNA processing. Proc. Natl. Acad. Sci. U S A *103*, 12707–12712.

Schuetze, S., Stenberg, P.E., and Kabat, D. (1993). The Ets-related transcription factor PU.1 immortalizes erythroblasts. Mol. Cell Biol. *13*, 5670–5678.

Tolhuis, B., Palstra, R.J., Splinter, E., Grosveld, F., and De Laat, W. (2002). Looping and interaction between hypersensitive sites in the active beta-globin locus. Mol. Cell *10*, 1453–1465.

Watowich, S.S. (2011). The erythropoietin receptor: molecular structure and hematopoietic signaling pathways. J. Invest. Med. *59*, 1067–1072.

Weintraub, A.S., Li, C.H., Zamudio, A.V., Sigova, A.A., Hannett, N.M., Day, D.S., Abraham, B.J., Cohen, M.A., Nabet, B., Buckley, D.L., et al. (2017). YY1 is a structural regulator of enhancer-promoter loops. Cell *171*, 1573–1588.e28.

Weiss, A.K.H., Naschberger, A., Loeffler, J.R., Gstach, H., Bowler, M.W., Holzknecht, M., Cappuccio, E., Pittl, A., Etemad, S., Dunzendorfer-Matt, T., et al. (2018). Structural basis for the bi-functionality of human oxaloacetate decarboxylase FAHD1. Biochem. J. *475*, 3561–3576.

Weiss, M.J., and Orkin, S.H. (1995). GATA transcription factors: key regulators of hematopoiesis. Exp. Hematol. *23*, 99–107.

Yao, L., Berman, B.P., and Farnham, P.J. (2015). Demystifying the secret mission of enhancers: linking distal regulatory elements to target genes. Crit. Rev. Biochem. Mol. Biol. *50*, 550–573.

Zhu, J., Adli, M., Zou, J.Y., Verstappen, G., Coyne, M., Zhang, X., Durham, T., Miri, M., Deshpande, V., De Jager, P.L., et al. (2013). Genome-wide chromatin state transitions associated with developmental and environmental cues. Cell *152*, 642–654.

iScience, Volume *23*

Supplemental Information

Erythropoietin Regulates Transcription and YY1 Dynamics in a Pre-established Chromatin Architecture

Andrea A. Perreault, Jonathan D. Brown, and Bryan J. Venters

Supplemental Information
Supplemental Figures and Legends

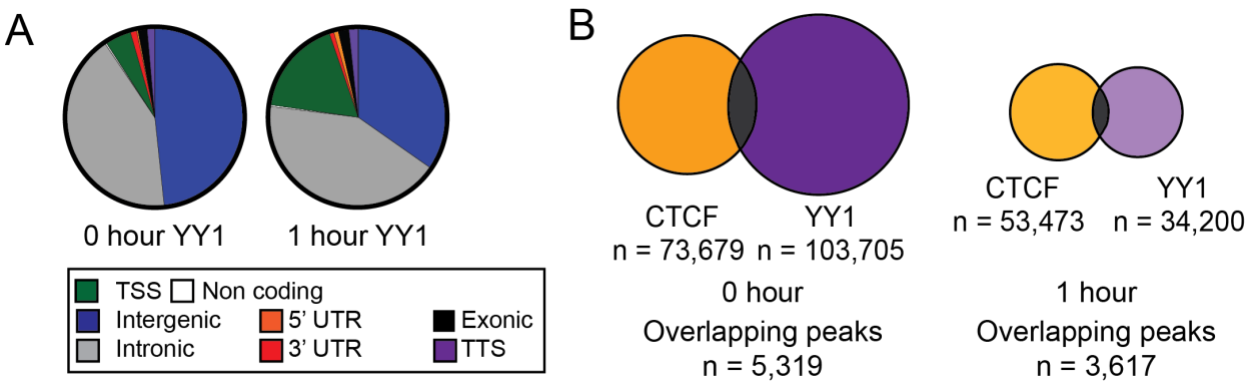

Figure S1. EPO dynamically regulates YY1 occupancy genome-wide, Related to Figure 3.
(A) YY1 binding locations in the genome.
(B) Comparison of CTCF and YY1 peak overlap before and after 1 hour EPO stimulation.

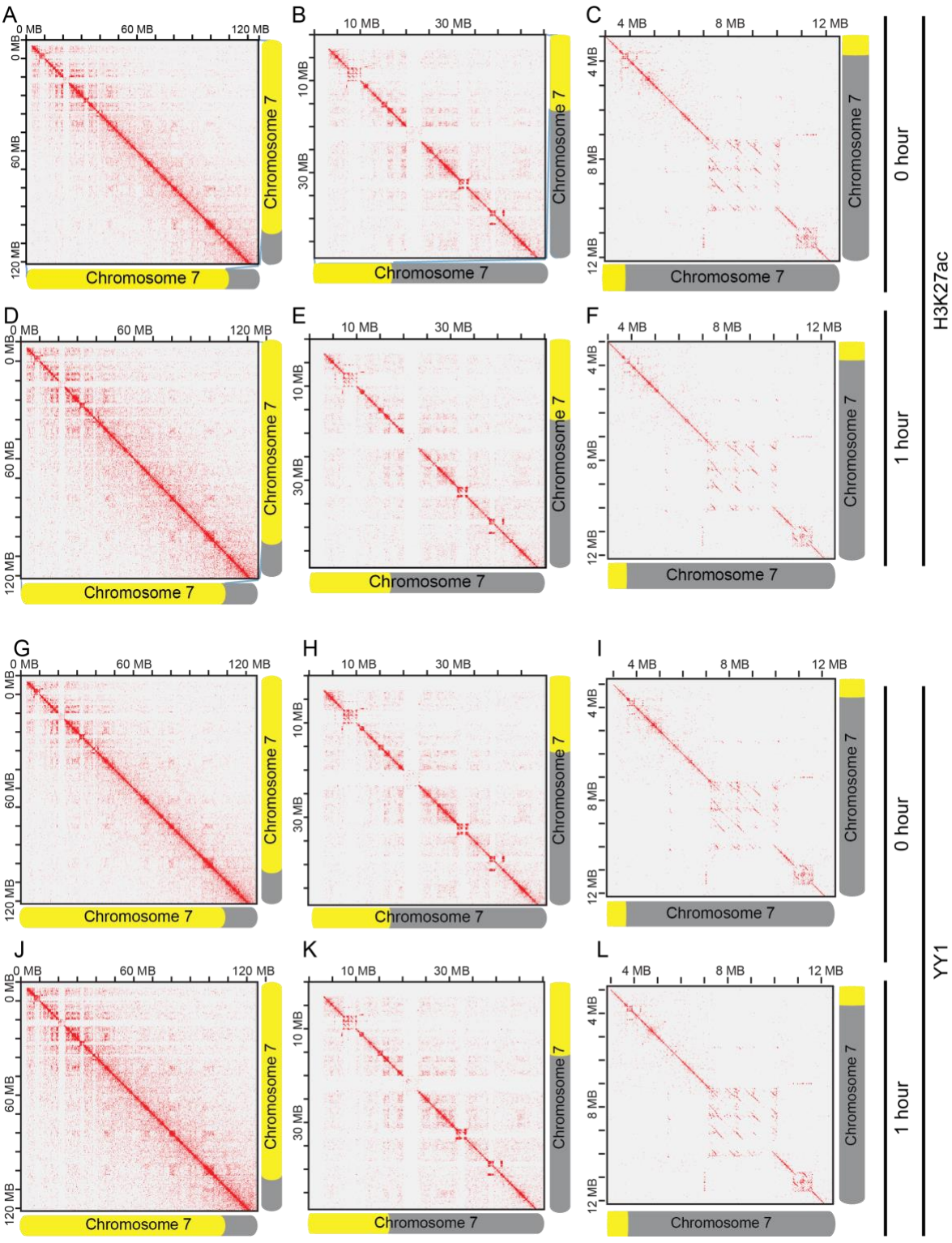

Figure S2. Representative chromatin contact maps for H3K27ac and YY1 HiChIP, Related to Figure 4.
Chromatin contacts mediated by H3K27ac at 0 hour EPO at (A) 250kb, (B) 100kb, and (C) 25kb resolutions.

Chromatin contacts mediated by H3K27ac at 1 hour EPO at (D) 250kb, (E) 100kb, and (F) 25kb resolutions.
Chromatin contacts mediated by YY1 at 0 hour EPO at (G) 250kb, (G) 100kb, and (I) 25kb resolutions.
Chromatin contacts mediated by YY1 at 1 hour EPO at (J) 250kb, (K) 100kb, and (L) 25kb resolutions.

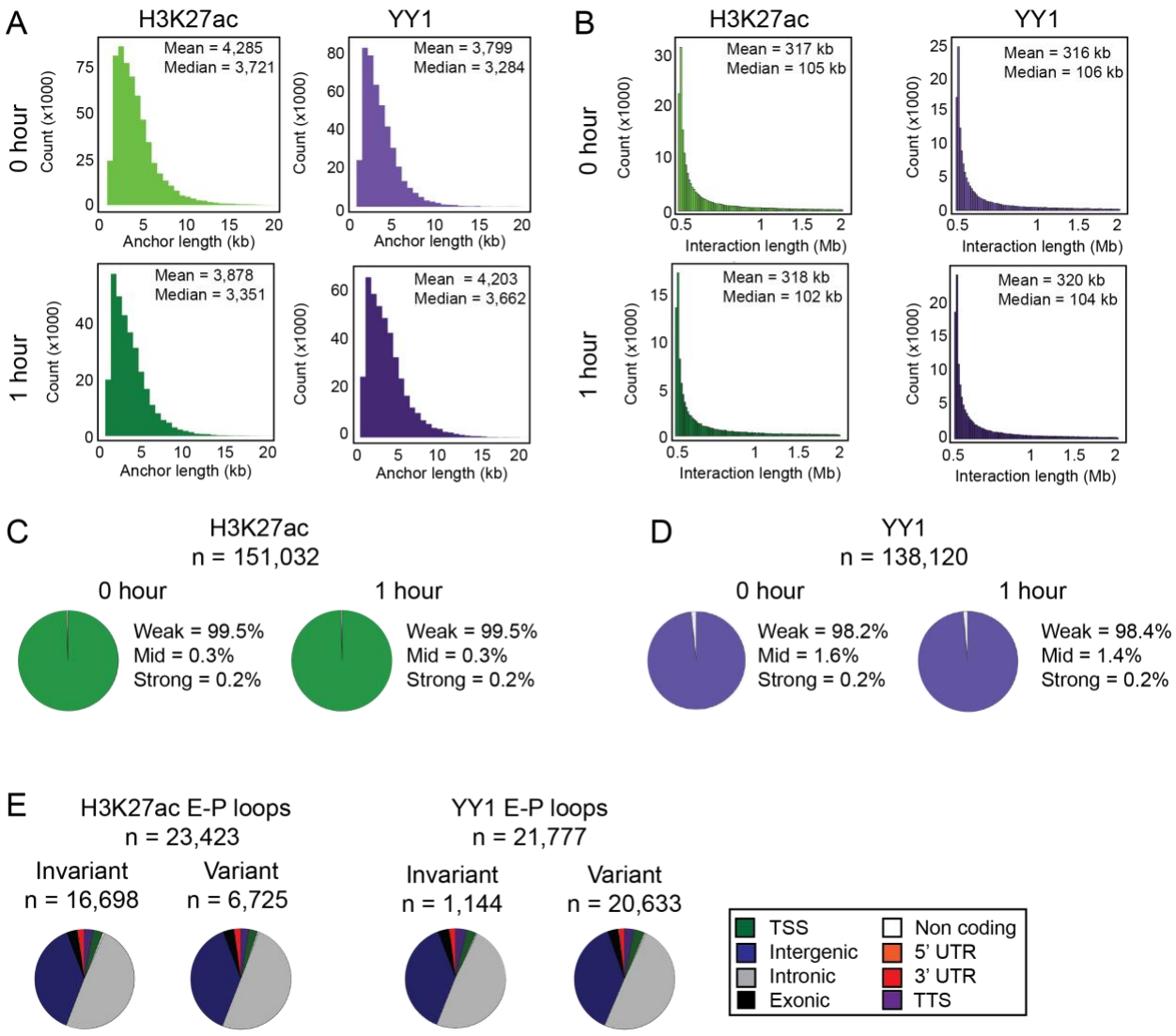

Figure S3. Characterization of chromatin loops mediated by H3K27ac and YY1, Related to Figure 4.

(A) Histogram showing the size distribution of anchors for HiChIP interactions in H3K27ac and YY1 libraries pre and post EPO stimulation.

(B) Histogram showing the size distribution of HiChIP interactions in H3K27ac and YY1 libraries pre and post EPO stimulation with log transformed x-axis.

(C) Fraction of weak (score < 5), moderate (score between 5 and 10), and strong (score > 10) H3K27ac chromatin interactions.

(D) Fraction of weak (score < 5), moderate (score between 5 and 10), and strong (score > 10) YY1 chromatin interactions.

(E) H3K27ac and YY1 enhancer-promoter (E-P) loops location in the genome.

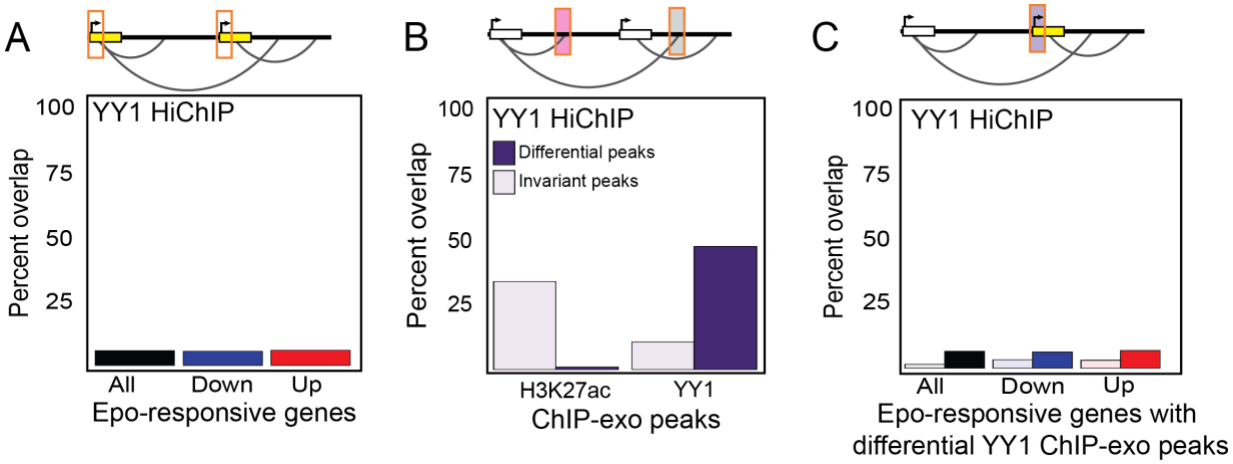

Figure S4. EPO regulates transcription in a pre-established chromatin conformation, Related to Figure 4.
(A) Proportion of interactions with promoters of EPO-responsive genes within YY1 HiChIP anchor regions.
(B) Proportion of interactions with differential H3K27ac or YY1 ChIP-exo peaks within anchor regions of YY1 HiChIP. Dark purple bars represent differential peaks TSS and light purple bars represent invariant peaks.
(C) Proportion of interactions with differential YY1 ChIP-exo peaks at promoters of EPO-responsive genes within YY1 HiChIP anchor regions. Dark bars represent EPO-responsive genes and light bars represent non-responsive genes.

Supplemental Tables

EPO (hr)	Total Reads	Reads Mapped	Mapping Rate	Unique Alignments	Unique Alignment Rate
0	51,086,988	46,916,946	92%	41,863,305	89%
	45,921,261	41,377,364	90%	37,200,184	90%
TOTAL	**97,008,249**	**88,294,310**		**79,063,489**	
1	43,417,043	39,605,767	91%	35,426,491	89%
	41,859,970	38,359,940	92%	34,287,633	89%
TOTAL	**85,277,013**	**77,965,707**		**69,714,124**	
4	45,650,667	42,564,629	93%	38,558,884	91%
	45,449,989	42,713,118	94%	38,620,867	90%
TOTAL	**91,100,656**	**85,277,747**		**77,179,751**	
12	48,350,536	44,651,856	92%	39,951,845	89%
	36,427,604	33,320,942	91%	29,800,144	89%
TOTAL	**84,778,140**	**77,972,798**		**69,751,989**	
24	49,732,518	43,101,597	87%	37,125,032	86%
	52,028,791	44,389,763	85%	38,266,645	86%
TOTAL	**101,761,309**	**87,491,360**		**75,391,677**	
36	40,613,328	33,511,866	83%	27,638,763	82%
	43,849,891	35,066,453	80%	28,300,690	81%
TOTAL	**84,463,219**	**68,578,319**		**55,939,453**	
Average Total Reads	**45,365,716**				
Average Mapped Reads		**40,465,020**			
Average Mapping Rate			**89%**		
Average Unique Alignments				**35,586,707**	
Average Unique Alignment Rate					**88%**

Table S1. RNA-seq sequencing statistics, Related to Figure 1.

Factor	Antibody	EPO (hr)	Total Reads	Uniquely Mapped	Unique Mapping Rate	Reads in Peaks	FRiP score
H3K27ac	ab4729	Previously published in Perreault, AA et al. (2017). Epo reprograms the epigenome of erythroid cells. *Experimental Hematology*. 51:47-62. Accession SRR4033061.					
RNA Pol II	sc-17798	0	23,599,539	18,845,128	80%		
			28,190,841	21,919,833	78%		
		TOTAL	**51,790,380**	**40,764,961**			
		1	25,380,733	19,181,745	76%		
			37,920,484	27,071,841	71%		
		TOTAL	**63,301,217**	**46,253,586**			
YY1	ab109237	0	49,303,713	32,145,330	65%		
			40,696,838	30,594,858	75%		
		TOTAL	**90,000,551**	**62,740,188**		8,881,135	0.141
		1	35,858,543	27,770,365	77%		
			43,771,372	32,777,027	75%		
		TOTAL	**79,629,915**	**60,547,392**		7,641,246	0.126
CTCF	07-729	0	53,987,299	45,182,628	84%		
			43,271,833	36,981,391	85%		
		TOTAL	**97,259,132**	**82,164,019**		40,119,395	0.488
		1	79,931,427	69,917,844	87%		
			37,329,553	30,956,490	83%		
		TOTAL	**117,260,980**	**100,874,334**		45,217,007	0.448
Average Total Reads			**41,603,515**				
Average Uniquely Mapped Reads				**32,778,707**			
Average Unique Mapping Rate					**77%**		

Table S2. ChIP-exo sequencing statistics, Related to Figure 2 and Figure 3.

Factor	Antibody	EPO (hr)	Pearson R Correlation
H3K27ac	ab4729	Previously published in Perreault, AA et al. (2017). Epo reprograms the epigenome of erythroid cells. *Experimental Hematology*. 51:47-62. Accession SRR4033061.	
RNA Pol II	sc-17798	0	0.80
		1	0.93
YY1	ab109237	0	0.97
		1	0.98
CTCF	07-729	0	0.97
		1	0.90

Table S3. ChIP-exo replicate correlation, Related to Figure 2 and Figure 3.

Factor	Antibody	EPO (hr)	Total Reads	Uniquely Mapped	Unique Mapping Rate
H3K27ac	ab4729	0	142,631,900	111,707,585	78%
			138,004,467	106,827,868	77%
		TOTAL	**280,636,367**	**218,535,453**	
		1	98,098,074	77,046,401	79%
			112,702,483	89,295,539	79%
		TOTAL	**210,800,557**	**166,341,940**	
YY1	ab109237	0	87,091,506	64,912,022	75%
			177,427,621	134,801,412	76%
		TOTAL	**264,519,127**	**199,713,434**	
		1	132,325,240	104,733,597	79%
			119,806,706	92,459,382	77%
		TOTAL	**252,131,946**	**197,192,979**	
Average Total Reads			**126,011,000**		
Average Uniquely Mapped Reads				**97,722,976**	
Average Unique Mapping Rate					**78%**

Table S4. HiChIP sequencing statistics, Related to Figure 4.

Factor	Antibody	EPO (hr)	Intra-chromosomal PETs	Long range interactions (5kb - 2Mb)	Percent intra-chromosomal PETs that are long range interactions	Chromatin loops (long range interactions between two ChIP anchors)	Percent of long range interactions that are chromatin loops
H3K27ac	ab4729	0	4,047,067	539,269	13%	110,994	21%
			3,007,741	236,596	8%	41,777	18%
		TOTAL	**7,054,808**	**775,865**		**152,771**	
		1	2,347,022	345,799	15%	33,399	10%
			2,684,603	222,089	8%	30,563	14%
		TOTAL	**5,031,625**	**567,888**		**63,962**	
YY1	ab109237	0	2,352,166	360,662	15%	34,018	9%
			4,594,705	389,653	8%	76,845	20%
		TOTAL	**6,946,871**	**750,315**		**110,863**	
		1	3,406,813	434,841	13%	72,080	17%
			3,096,245	243,649	8%	29,769	12%
		TOTAL	**6,503,058**	**678,490**		**101,849**	
Average intrachromosomal PETS			**3,192,045**				
Average long range interactions				**346,570**			
Average percent of long range interactions					**11%**		
Average chromatin loops						**53,681**	
Average percent of chromatin loops							**15%**

Table S5. HiChIP chromatin interaction statistics, Related to Figure 4.

Factor	Antibody	EPO (hr)	Pearson R Correlation
H3K27ac	ab4729	0	0.92
		1	0.98
YY1	ab109237	0	0.96
		1	0.98

Table S6. HiChIP chromatin interaction replicate correlation, Related to Figure 4.

Transparent Methods

REAGENT or RESOURCE	SOURCE	IDENTIFIER
Antibodies		
RNA Pol II	Santa Cruz	Cat# sc-17798
H3K27ac	Abcam	Cat# ab4729
YY1	Abcam	Cat# ab109237
CTCF	Millipore	Cat# 07-729
Bacterial and Virus Strains		
Friend Virus	Mark Koury lab	N/A
Critical Commercial Assays		
Qubit dsDNA High Sensitivity kit	Invitrogen	Cat# Q32854
Zymo DNA Clean and Concentrator kit	Zymo	Cat# D4003
Qiagen RNAeasy kit	Qiagen	Cat# 74104
NEBNext Ultra II Directional DNA library preparation kit	Illumina	Cat# E75530S
Deposited Data		
Raw and analyzed data	This study	GSE142006
Enhancer annotation	(Perreault et al., 2017)	SRP082181
Mouse reference genome, NCBI build GRCm38/mm10	Genome Reference Consortium	https://www.ncbi.nlm.nih.gov/grc/mouse
Experimental Models: Organisms/Strains		
Mouse: Female BALB/cJ, 12 weeks	The Jackson Laboratory	
Software and Algorithms		
BWA-MEM	(Li and Durbin, 2010)	http://bio-bwa.sourceforge.net
Samtools	(Li et al., 2009)	http://samtools.sourceforge.net
HOMER	(Heinz et al., 2010)	http://homer.ucsd.edu/homer/
deepTOOLS	(Ramirez et al., 2014)	https://deeptools.readthedocs.io/en/develop/
BEDTools	(Quinlan, 2014)	https://bedtools.readthedocs.io/en/latest/
IGV	(Robinson et al., 2011)	https://software.broadinstitute.org/software/igv/
WashU Epigenome Browser	(Zhou et al., 2011)	http://epigenomegateway.wustl.edu
HiC-Pro	(Servant et al., 2015)	https://github.com/nservant/HiC-Pro

hichipper	(Lareau and Aryee, 2018b)	https://github.com/aryeelab/hichipper
Juicer	(Durand et al., 2016)	https://github.com/aidenlab/juicer/wiki/Juicer-Tools-Quick-Start
diffloop	(Lareau and Aryee, 2018a)	https://bioconductor.org/packages/release/bioc/html/diffloop.html
TopHat	(Trapnell et al., 2009)	https://ccb.jhu.edu/software/tophat/index.shtml
Cufflinks	(Trapnell et al., 2012)	http://cole-trapnell-lab.github.io/cufflinks/
cummeRbund		http://compbio.mit.edu/cummeRbund/ R package version 2.26.0
R		https://www.r-project.org
edgeR	(Robinson et al., 2010)	https://bioconductor.org/packages/release/bioc/html/edgeR.html
MACS	(Zhang et al., 2008)	https://github.com/taoliu/MACS

EXPERIMENTAL MODEL AND SUBJECT DETAILS

Isolation of Proerythroblasts from FVA infected mice

Highly purified proerythroblasts were obtained from spleens of mice infected with the Friend virus as previously described(Sawyer et al., 1987, Koury et al., 1984), with the following modifications. All animal procedures were performed in compliance with and approval from the Vanderbilt Division of Animal Care (DAC) and Institutional Animal Care and Use Committee (IACUC). Female BALB/cJ mice (12 weeks old, Jackson Laboratories) were infected via intraperitoneal injection of ~10_4 spleen focus-forming units of Anemia-inducing strain of the Friend virus (FVA). At 13 to 15 days post-infection, the mice were sacrificed and spleens removed. The spleens were homogenized to a single cell suspension by passing the minced spleens through a sterile 100 micron nylon mesh filter into sterile solution of 0.2% bovine serum albumin (BSA) in 1x PBS. The filtrate was then repeatedly pipetted to ensure a single cell suspension. The homogenized spleen cells were size-separated by gravity sedimentation for 4 hours at 4°C in a continuous gradient of 1% to 2% deionized BSA.

The sedimentation apparatus consisted of a 25cm diameter sedimentation chamber containing a 2.4L BSA gradient, two BSA gradient chambers containing 1.2L 1% and 2% deionized BSA in 1x PBS, and a cell loading chamber (ProScience Inc.) containing the 50ml cell suspension. After 4 hour sedimentation, cells were collected in 50ml fractions, with proerythroblasts typically enriched in fractions 5-20 of 24 total fractions. Typically about 10^9 proerythroblasts were obtained from the separation of 10^{10} nucleated spleen cells (6-7g spleen weight) across three 25cm sedimentation chambers.

Cell Culture Conditions

To study the effects of erythropoietin (EPO) on terminal erythroid differentiation, FVA-derived proerythroblasts were cultured at 10^6 cells/ml in Iscove-modified Dulbecco medium (IMDM, Life Technologies #12440043), 30% heat-inactivated fetal bovine serum (Gibco, 26140-079), 1% Penicillin-Streptomycin (Gibco #15140-122), 10% deionized BSA, and 100uM alpha-thioglycerol (MP Biomedicals #155723). Terminal erythroid differentiation of purified proerythroblasts was induced by the addition of 0.4 U/ml human recombinant EPO (10kU/ml Epogen by Amgen, NDC 55513-144-10) to media. At the desired times after the addition of EPO, cells were crosslinked by the addition of 1% formaldehyde for 10 minutes for ChIP analysis and 2% formaldehyde for 20 minutes for HiChIP analysis. Crosslinking was then quenched by the addition of 125mM glycine. Crosslinked cells were collected by centrifugation for 5 minutes at 1,000g at 4°C, washed once with 1x PBS, flash frozen in liquid nitrogen, and stored at -80°C until used. For RNA-seq, cells were removed from culture before crosslinking. Samples were spun for 5 minutes at 1,000g at 4°C and the supernatant was aspirated. Pellets were flash frozen in liquid nitrogen and stored at -80°C until used.

EXPERIMENTAL DESIGN

All experiments were replicated. No aspect of the study was done blinded. Sample size was not predetermined.

HiChIP

HiChIP was performed as described(Mumbach et al., 2016) with a few modifications.

In Situ Contact Generation

50 million cell pellets were resuspended in 2.5ml ice cold Hi-C Lysis Buffer (10mM Tris HCl, 10mM NaCl, 0.2% NP-40, 1X protease inhibitors (Roche, 04693124001)) and split into 10 million cell amounts. Samples were incubated at 4°C for 30 minutes with rotation. Nuclei were pelleted by centrifugation at 2,500g for 5 minutes at 4°C and washed once with 500ul of ice cold Hi-C Lysis Buffer. After removing supernatant, nuclei were resuspended in 100ul of 0.5% SDS and incubated at 62°C for 10 minutes. SDS was quenched by adding 285ul water and 50ul 10% Triton X-100. Samples were vortexed and incubated for 15 minutes at 37°C. After the addition of 50ul of 10X NEBBuffer 2 (NEB, B7002) and 1ul of MboI restriction enzyme (NEB, R0147), chromatin was digested at 37°C for 1 hour at 700rpm on Thermomixer. Following digestion, MboI enzyme was heat inactivated by incubating the nuclei at 62°C for 20

minutes. To fill in the restriction fragment overhangs and mark the DNA ends with biotin, 52ul of fill-in master mix, containing 15ul of 1mM biotin-dATP (Jena BioScience, NU-835-BIO14-L), 1.5ul of 10mM dCTP (NEB, N044_S), 1.5ul of 10mM dGTP (NEB, N044_S), 1.5ul of 10mM dTTP (NEB, N044_S), and 10ul of 5 U/ul DNA Polymerase I, Large (Klenow) Fragment (NEB, M0210), was added and the tubes were incubated at 37°C for 1 hour at 700rpm on Thermomixer. Proximity ligation was performed by addition of 948ul of ligation master mix, containing 150ul of 10X NEB T4 DNA ligase buffer (NEB, B0202), 125ul of 10% Triton X-100, 15ul of 10 mg/mL BSA (NEB, B9000), 10ul of 400 U/mL T4 DNA ligase (NEB, M0202), and 648ul of water, and incubation at room temperature for 4 hours with rotation.

Sonication and Chromatin Immunoprecipitation

After proximity ligation, nuclei were pelleted by centrifugation at 2500g for 5 minutes and resuspended in 880ul Nuclear Lysis Buffer (50mM Tris HCl, 10mM EDTA, 1% SDS, 1X protease inhibitors (Roche, 04693124001)). Samples were vortexed and nuclei were sonicated with a Bioruptor (Diagenode) for 10 minutes on the low setting to solubilize chromatin. Sonicated chromatin was clarified by centrifugation at 16,100g for 15 min at 4°C and supernatant from 10 million cell samples are pooled to a total of 50 million cells. Sample was diluted with 2X ChIP Dilution Buffer (0.01% SDS, 1.1% Triton X-100, 1.2mM EDTA, 16.7mM Tris HCl, 167mM NaCl). 300ul Protein A beads (Thermo, 21348) were washed in 2ml ChIP Dilution Buffer and resuspended in 250ul ChIP Dilution Buffer. Beads were added to 50 million cell sample and incubated at 4°C for 1 hour with rotation. Beads were then separated on a magnetic rack and supernatant was transferred to a new tube. 10ug of antibody for Pol II (Santa Cruz, sc-17798), H3K27ac (Abcam, ab4729), or YY1 (Abcam, ab109237) were added to the tube. Samples were incubated overnight at 4°C with rotation. The next day, 300ul Protein A beads were washed in 2ml ChIP Dilution Buffer and resuspended in 500ul ChIP Dilution Buffer. Beads were added to 50 million cell sample with antibody and incubated at 4°C for 2 hours with rotation. Beads were then separated on a magnetic rack and washed three times with 750ul Low Salt Wash Buffer (0.1% SDS, 1% Triton X-100, 2mM EDTA, 20mM Tris HCl, 150mM NaCl), three times with 750ul High Salt Wash Buffer (0.1% SDS, 1% Triton X-100, 2mM EDTA, 20mM Tris HCl, 500mM NaCl), and three times with 750ul LiCl Wash Buffer (10mM Tris HCl, 250mM LiCl, 1% NP-40, 1% Na-Doc, 1mM EDTA).

DNA Elution and Reverse Crosslinking

Beads were then resuspended in 200ul of DNA Elution Buffer (50mM $NaHCO_3$, 1% SDS), which is made fresh, and incubated at room temperature for 10 minutes with rotation, followed by 37°C for 3 minutes at 700rpm. Samples were placed on a magnetic rack and supernatant transferred to a new tube. This was repeated once more. 10ul of Proteinase K (Roche, 03115828001) was added to each tube and samples were incubated at 55°C for 45 minutes at 700rpm, followed by 67°C for 1.5 hours at 700rpm. DNA was then purified using Zymo DNA Clean and Concentrator (Zymo, D4003) according to manufacturer's protocol and eluted in 10ul water. The amount of eluted DNA was quantified by Qubit dsDNA HS kit (Invitrogen, Q32854).

Biotin Capture and Sequencing Preparation

25ul of Streptavidin C-1 beads (Invitrogen, 65001) were washed with 1ml Tween Wash Buffer (5MM Tris HCl, 0.5mM EDTA, 1M NaCl, 0.05% Tween-20) and resuspended in

10ul of 2X Biotin Binding Buffer (10mM Tris HCl, 1mM EDTA, 2M NaCl). 10ul of bead mixture was added to 50ng of purified DNA for each sample, incubating at room temperature for 15 minutes, agitating every 5 minutes. After capture, beads were separated with a magnet and the supernatant was discarded. Beads were then washed twice with 500ul of Tween Wash Buffer, incubating at 55°C for 2 minutes at 700rpm. Beads were washed with 100ul 1X TD Buffer (diluted from 2X TD Buffer (20mM Tris HCl, 10mM $MgCl_2$, 20% Dimethylformamide)). Beads were resuspended in 50ul of master mix, containing 25ul 2X TD Buffer, 2.5ul Tn5 Tagment DNA enzyme (Illumina, 15027865), and 22.5ul water. Samples were incubated at 55°C for 10 minutes at 700rpm. Beads were separated on a magnet and supernatant was discarded. Beads were washed with 750ul of 50mMEDTA at 50°C for 30 minutes, washed twice with 750ul of 50mMEDTA at 50°C for 3 minutes each, then washed twice with 750ul of Tween Wash Buffer at 55°C for 2 minutes each, and finally washed once with 750uL of 10mM Tris HCl pH 7.5. Beads were separated on a magnet and supernatant was discarded.

PCR and Size Selection

To generate the sequencing library, PCR amplification of the tagmented DNA was performed while the DNA is still bound to the beads. Beads were resuspended in a PCR master mix, consisting of 36ul water, 1.25 unique Nextera Ad2.X primer, 10ul Phusion HF 5X buffer (NEB, E0553), 1ul 10mM dNTPs, 1.25ul universal Nextera Ad1 primer, and 0.5ul Phusion DNA Polymerase (NEB, E0553). DNA was amplified with 8 cycles of PCR. After PCR, beads were separated on a magnet and the supernatant containing the PCR amplified library was transferred to a new tube, purified using the Zymo DNA Clean and Concentrator (Zymo D4003) kit according to manufacturer's protocol and eluted in 52ul water. Purified HiChIP libraries were size selected to 300-700 basepairs using a double size selection with AMPure XP beads (Beckman Coulter, A68831). HiChIP libraries were paired-end sequenced on an Illumina NextSeq500 with reads 75 nucleotides in length.

Chromatin Immunoprecipitation with Lambda Exonuclease Digestion (ChIP-exo)

With the following modifications, ChIP-exo was performed as previously described(Perreault and Venters, 2016, Rhee and Pugh, 2011) with chromatin extracted from 50 million cells, ProteinG MagSepharose resin (GE Healthcare), and 10ug of antibody directed against Pol II (Santa Cruz, sc-17798), YY1 (Abcam, ab109237), or CTCF (Millipore, 07-729). First, formaldehyde crosslinked cells were lysed with buffer 1 (50mM HEPES–KOH pH 7.5, 140mM NaCl, 1 mM EDTA, 10% Glycerol, 0.5% NP-40, 0.25% Triton X-100), washed once with buffer 2 (10mM Tris HCL pH 8, 200mM NaCl, 1mM EDTA, 0.5mM EGTA), and the nuclei lysed with buffer 3 (10mM Tris HCl pH 8, 100mM NaCl, 1mM EDTA, 0.5mM EGTA, 0.1% Na–Deoxycholate, 0.5% *N*-lauroylsarcosine). All cell lysis buffers were supplemented with fresh EDTA-free complete protease inhibitor cocktail (CPI, Roche #11836153001). Purified chromatin was sonicated with a Bioruptor (Diagenode) to obtain fragments with a size range between 100 and 500 base pairs. Triton X-100 was added to extract at 1% to neutralize sarcosine. Insoluble chromatin debris was removed by centrifugation, and sonication extracts stored at -80°C until used for ChIP analysis. Libraries were sequenced using an

Illumina NextSeq500 sequencer as single-end reads 75 nucleotides in length on high output mode.

RNA-seq

RNA was isolated using the Qiagen RNAeasy kit (Qiagen, 74104) per manufacturer's instructions. Stranded polyA selected libraries were prepared using NEBNext PolyA mRNA isolation standard protocol, NEBNext rRNA Depletion standard protocol, and finally NEBNext Ultra II Directional DNA library preparation kit (Illumina, E75530S) per manufacturer's protocol. PCR amplified RNA-seq libraries were size selected using AMPure XP beads (Beckman Coulter, A68831). RNA-seq libraries were subjected to 75 basepair single end sequencing on Illumina NextSeq500 sequencer.

QUANTIFICATION AND STATISTICAL ANALYSIS

HiChiP data analysis

Alignment

HiChIP library sequence reads were aligned to the mouse mm10 reference genome using HiC-Pro(Servant et al., 2015) with the following options in the configuration file:

```
BOWTIE2_OPTIONS = --very-sensitive --end-to-end –reorder
LIGATION_SITE = GATCGATC
GET_ALL_INTERACTION_CLASSES = 1
GET_PROCESS_SAM = 1
RM_SINGLETON = 1
RM_MULTI = 1
RM_DUP = 0
```

Use of replicates

Biological replicates were run through HiC-Pro in parallel. Replicate correlation was assessed after HiC-Pro processing. Specifically, .allValidPairs files were compared using Pearson's correlation test. R values can be found in Supplemental Table 6.

Chromatin interaction identification

Hichipper(Lareau and Aryee, 2018b) was applied to HiC-Pro output files to identify high confidence chromatin contacts using EACH, ALL peak finding settings. Interaction calls for each replicate are considered individually for loop analysis and annotation in hichipper. The quickAssoc and annotateLoops functions in the diffloop R package(Lareau and Aryee, 2018a) were used to find differential loops and annotate epigenetic features, respectively. Enhancers were denoted as the intersection of H3K4me1 and H3K27ac peaks (previously published data) and promoters were identified using the getMouseTSS function.

HiChIP display

To visualize chromatin interactions identified using HiChIP, the –make-ucsc option was added when analyzing the data using hichipper(Lareau and Aryee, 2018b).

ChIP-exo data analysis

Alignment

ChIP-exo library sequence reads were aligned to the mouse mm10 reference genome using BWA-MEM algorithm(Li and Durbin, 2010) using default parameters. The resulting bam files were first sorted using the Samtools Sort function(Li et al., 2009), and then bam index files were generated using the Samtools Index function(Li et al., 2009).

Peak calling

ChIP-exo peaks were annotated and quantified using the Hypergeometric Optimization of Motif EnRichment (HOMER) suite(Heinz et al., 2010). Briefly, bam files were converted to tag directories using the makeTagDirectory function with the –genome, –checkGC, and –format options. The findPeaks function was used to identify ChIP peaks using –o auto and –style gro-seq or factor for Pol II or CTCF/YY1 libraries, respectively. To quantify and normalize tags to RPKM, the analyzeRepeats function was used with the –rpkm, –count genes, –strand both, –condenseGenes, and –d options.

Use of replicates

Replicate correlation was assessed after peak calling. Specifically, RPKM calculated from analyzeRepeats function were plotted using scatterplot compared using Pearson's correlation test. R values can be found in Supplementary Table 3. Replicates were merged for final analyses presented in the manuscript.

Heatmaps

bigWig files for CTCF and YY1 libraries were generated using the deepTools bamCoverage function(Ramirez et al., 2014). To create aligned heatmaps, first a matrix was generated using the computeMatrix function with the following options: reference-point –S, –a 2000, –b 2000, -–referencePoint center, –verbose, –missingDataAsZero, and –p max/2. Then, the heatmap was created using the plotHeatmap function with the following options: –verbose and –sortRegions descend.

ChIP-exo display

Raw sequencing tags were smoothed (20 basepair bin, 100 basepair sliding window) and normalized to reads per kilobase per million (RPKM) using deepTOOLS(Ramirez et al., 2014) and visualized with Integrative Genomics Viewer (IGV)(Robinson et al., 2011).

RNA-seq data analysis

RNA-seq alignment, transcript assembly, and differential expression

RNA-seq library sequence reads were aligned to the mouse mm10 reference genome using TopHat(Trapnell et al., 2009) using default parameters. Cufflinks(Trapnell et al., 2012) was used to assemble transcripts and quantify expression of transcripts. Cuffmerge(Trapnell et al., 2012) merges all transcript assemblies to create a single merged transcriptome annotation for final analyses. The program conducts multiple hypothesis correction and calculates an adjusted FDR q-value.

Use of replicates

Replicates are both used as input for the cufflinks and cuffmerge programs described above.

RNA-seq display

CummeRbund visualizes RNA-seq data analyzed using cufflinks.

Definition of regulatory regions

Throughout the manuscript multiple analyses rely on overlaps with different regulatory regions, namely enhancers and promoters. Here we explain how these regulatory regions were defined.

Promoters are defined here as the comprehensive list of annotated transcription start sites (TSS) in the mm10 mouse genome from UCSC.

Enhancers are defined here as regions of the genome marked by H3K4me1 and H3K27ac. This group is further supported by enhancer identified using ChromHMM in (Perreault et al., 2017).

Definition of chromatin features

Throughout the manuscript multiple analyses rely on overlaps with different chromatin features. Here we explain how these features were defined.

HiChIP anchors, as identified by the hichipper analysis pipeline, are the regions between restriction enzyme motifs that contain a ChIP peak for the factor of interest by extending ChIP peaks to the edges of the restriction fragment. As a consequence of this computational definition, HiChIP anchors typically span a wide range of lengths. In the present study, we use anchor as a broad term to define the endpoints of a HiChIP loop.

HiChIP loops are defined as the distance between two ends of a chromatin interaction called anchors, which are identified in hichipper. These loops have a specific score, which is the number of paired-end tags (PETs) that support the interaction. In this study, we separate loops into 3 categories (weak, moderate, and strong) based on the interquartile range of the loop scores determined by diffloop.

Invariant loops are chromatin interactions that satisfy two criteria. First, these loops have a fold change in score (as calculated by diffloop) to be between -2 and 2. A fold change of +/-2 is commonly used in the literature to separate variant and invariant features and was used here as a continuation of our previously published work. Second, FDR > 0.1 (as calculated by diffloop). Usually FDR < 0.1 would subset the group of chromatin loops that are significantly different between two conditions. Therefore, the complement of this group is the subset of chromatin loops that are not significantly different.

Supplemental References

DURAND, N. C., SHAMIM, M. S., MACHOL, I., RAO, S. S., HUNTLEY, M. H., LANDER, E. S. & AIDEN, E. L. 2016. Juicer Provides a One-Click System for Analyzing Loop-Resolution Hi-C Experiments. *Cell Syst,* 3**,** 95-8.

HEINZ, S., BENNER, C., SPANN, N., BERTOLINO, E., LIN, Y. C., LASLO, P., CHENG, J. X., MURRE, C., SINGH, H. & GLASS, C. K. 2010. Simple combinations of lineage-determining transcription factors prime cis-regulatory elements required for macrophage and B cell identities. *Mol Cell,* 38**,** 576-89.

KOURY, M. J., SAWYER, S. T. & BONDURANT, M. C. 1984. Splenic erythroblasts in anemia-inducing Friend disease: a source of cells for studies of erythropoietin-mediated differentiation. *Journal of cellular physiology,* 121**,** 526-32.

LAREAU, C. A. & ARYEE, M. J. 2018a. diffloop: a computational framework for identifying and analyzing differential DNA loops from sequencing data. *Bioinformatics,* 34**,** 672-674.

LAREAU, C. A. & ARYEE, M. J. 2018b. hichipper: a preprocessing pipeline for calling DNA loops from HiChIP data. *Nat Methods,* 15**,** 155-156.

LI, H. & DURBIN, R. 2010. Fast and accurate long-read alignment with Burrows-Wheeler transform. *Bioinformatics,* 26**,** 589-95.

LI, H., HANDSAKER, B., WYSOKER, A., FENNELL, T., RUAN, J., HOMER, N., MARTH, G., ABECASIS, G., DURBIN, R. & GENOME PROJECT DATA PROCESSING, S. 2009. The Sequence Alignment/Map format and SAMtools. *Bioinformatics,* 25**,** 2078-9.

MUMBACH, M. R., RUBIN, A. J., FLYNN, R. A., DAI, C., KHAVARI, P. A., GREENLEAF, W. J. & CHANG, H. Y. 2016. HiChIP: efficient and sensitive analysis of protein-directed genome architecture. *Nat Methods,* 13**,** 919-922.

PERREAULT, A. A., BENTON, M. L., KOURY, M. J., BRANDT, S. J. & VENTERS, B. J. 2017. Epo reprograms the epigenome of erythroid cells. *Exp Hematol*.

PERREAULT, A. A. & VENTERS, B. J. 2016. The ChIP-exo Method: Identifying Protein-DNA Interactions with Near Base Pair Precision. *J Vis Exp*.

QUINLAN, A. R. 2014. BEDTools: The Swiss-Army Tool for Genome Feature Analysis. *Curr Protoc Bioinformatics,* 47**,** 11 12 1-11 12 34.

RAMIREZ, F., DUNDAR, F., DIEHL, S., GRUNING, B. A. & MANKE, T. 2014. deepTools: a flexible platform for exploring deep-sequencing data. *Nucleic Acids Res,* 42**,** W187-91.

RHEE, H. S. & PUGH, B. F. 2011. Comprehensive genome-wide protein-DNA interactions detected at single-nucleotide resolution. *Cell,* 147**,** 1408-19.

ROBINSON, J. T., THORVALDSDOTTIR, H., WINCKLER, W., GUTTMAN, M., LANDER, E. S., GETZ, G. & MESIROV, J. P. 2011. Integrative genomics viewer. *Nat Biotechnol,* 29**,** 24-6.

ROBINSON, M. D., MCCARTHY, D. J. & SMYTH, G. K. 2010. edgeR: a Bioconductor package for differential expression analysis of digital gene expression data. *Bioinformatics,* 26**,** 139-40.

SAWYER, S. T., KOURY, M. J. & BONDURANT, M. C. 1987. Large-scale procurement of erythropoietin-responsive erythroid cells: assay for biological activity of erythropoietin. *Methods Enzymol,* 147**,** 340-52.

SERVANT, N., VAROQUAUX, N., LAJOIE, B. R., VIARA, E., CHEN, C. J., VERT, J. P., HEARD, E., DEKKER, J. & BARILLOT, E. 2015. HiC-Pro: an optimized and flexible pipeline for Hi-C data processing. *Genome Biol,* 16**,** 259.

TRAPNELL, C., PACHTER, L. & SALZBERG, S. L. 2009. TopHat: discovering splice junctions with RNA-Seq. *Bioinformatics,* 25**,** 1105-11.

TRAPNELL, C., ROBERTS, A., GOFF, L., PERTEA, G., KIM, D., KELLEY, D. R., PIMENTEL, H., SALZBERG, S. L., RINN, J. L. & PACHTER, L. 2012. Differential gene and transcript expression analysis of RNA-seq experiments with TopHat and Cufflinks. *Nat Protoc,* 7**,** 562-78.

ZHANG, Y., LIU, T., MEYER, C. A., EECKHOUTE, J., JOHNSON, D. S., BERNSTEIN, B. E., NUSBAUM, C., MYERS, R. M., BROWN, M., LI, W. & LIU, X. S. 2008. Model-based analysis of ChIP-Seq (MACS). *Genome Biol,* 9**,** R137.

ZHOU, X., MARICQUE, B., XIE, M., LI, D., SUNDARAM, V., MARTIN, E. A., KOEBBE, B. C., NIELSEN, C., HIRST, M., FARNHAM, P., KUHN, R. M., ZHU, J., SMIRNOV, I., KENT, W. J., HAUSSLER, D., MADDEN, P. A., COSTELLO, J. F. & WANG, T. 2011. The Human Epigenome Browser at Washington University. *Nat Methods,* 8**,** 989-90.